

1 **Tracer-based source apportioning of atmospheric organic carbon and**  
2 **the influence of anthropogenic emissions on secondary organic aerosol**  
3 **formation in Hong Kong**

4 Yubo Cheng<sup>1</sup>, Yiqiu Ma<sup>1,2</sup>, Di Hu<sup>1,2</sup>

5 <sup>1</sup>State Key Laboratory of Environmental and Biological Analysis, Department of Chemistry, Hong Kong Baptist University,  
6 Kowloon Tong, Kowloon, Hong Kong, P. R. China

7 <sup>2</sup>HKBU Institute of Research and Continuing Education, Shenzhen Virtual University Park, Shenzhen, 518057, P. R. China

8 *Correspondence to:* Di Hu ([dihu@hkbu.edu.hk](mailto:dihu@hkbu.edu.hk))

9 **Abstract.** Here we conducted comprehensive chemical characterization and source apportionment of 49 PM<sub>2.5</sub> samples  
10 collected in Hong Kong. Besides the major aerosol constituents, 39 polar organic species, including 14 secondary organic  
11 aerosol (SOA) tracers of isoprene, monoterpenes,  $\beta$ -caryophyllene, and naphthalene, were quantified using gas  
12 chromatography-mass spectrometry (GC-MS). Six factors, i.e., SOA, secondary sulfate (SS), biomass burning (BB)/SOA, sea  
13 salt, marine vessels, and vehicle emissions, were apportioned by positive matrix factorization (PMF) as the major sources of  
14 ambient organic carbon (OC) in Hong Kong. The secondary formation, including OC from SOA, SS, and aging of BB plume,  
15 was the leading contributor to OC (51.4%,  $2.15 \pm 1.37 \mu\text{gC m}^{-3}$ ) throughout the year. We then applied a tracer-based method  
16 (TBM) to estimate the SOA formation from the photo-oxidation of four selected precursors, and monoterpenes SOA was the  
17 most abundant. A Kintecus kinetic model was used to examine the formation channels of isoprene SOA, and the aerosol-phase  
18 ring-opening reaction of isoprene epoxydiols (IEPOX) was found to be the dominant formation pathway. Consistently, IEPOX  
19 tracers contributed 94% of total GC-MS quantified isoprene SOA tracers. The TBM-estimated secondary organic carbon SOC  
20 ( $\text{SOC}_{\text{TBM}}$ ) and PMF-resolved SOC ( $\text{SOC}_{\text{PMF}}$ ) showed similar temporal trends; however,  $\text{SOC}_{\text{TBM}}$  only accounted for 26.5% of  
21  $\text{SOC}_{\text{PMF}}$ , indicating a large fraction of ambient SOA was from other reaction pathways/precursors. Results of Pearson's R and  
22 multivariate linear regression analysis showed that NO<sub>x</sub> processing played a key role in both daytime and nighttime SOA  
23 production in the region. ~~SOA formation through nighttime NO<sub>3</sub> oxidation of biogenic VOCs, especially monoterpenes, may~~  
24 ~~have made a considerable contribution to the SOA loading in Hong Kong.~~ Moreover, sulfate had a significant positive linear  
25 relationship with  $\text{SOC}_{\text{PMF}}$  and SS-related SOC, and particle acidity was significantly correlated with SOC from the aging of  
26 BB.

## 27 1 Introduction

28 Organic aerosol (OA) is a significant component of ambient fine particulate matter (PM<sub>2.5</sub>). It accounts for 20%-60% of the  
29 total PM<sub>2.5</sub> mass on a global scale (Kanakidou et al., 2005; Van Dingenen et al., 2004; Zhang et al., 2007), and even up to 90%  
30 in rural areas (Kanakidou et al., 2005; Roberts et al., 2001; Zhang et al., 2007). OA is either directly emitted into the atmosphere  
31 from natural (e.g., vegetative detritus, volcano activity) and anthropogenic sources (e.g., biomass burning (BB), vehicle  
32 exhaust, and cooking), or secondarily formed through the oxidation of biogenic and anthropogenic gas-phase precursors and  
33 the subsequent partition process or particle-phase reactions (Gelencsér et al., 2007; Hildemann et al., 1996; Hu et al., 2010;  
34 Zheng et al., 2014). Given the varying emission sources, meteorological conditions, and anthropogenic activities worldwide  
35 and their influences on ambient OA composition, aerosol scientists have put many efforts to investigate the atmospheric  
36 processes of OA and their primary and secondary sources, which aid the development of more targeted control policy of PM<sub>2.5</sub>  
37 pollution (Hu et al., 2010; Huang et al., 2014; Schauer et al., 2007; Simoneit, 1999; Stone et al., 2009; Zheng et al., 2005).  
38 Huang et al. (2014) applied positive matrix factorization (PMF) to apportion the sources of OA at four urban locations in China,

39 i.e., Beijing, Shanghai, Guangzhou, and Xi'an. They found that secondary formation accounted for a predominant fraction of  
40 OA (44-71%) at all four sites. Hong Kong, a megacity located on the southern coast of China in the PRD region and a hub port  
41 for the South Asian Pacific region, has its unique OC source characteristics. Hu et al. (2010) incorporated biogenic and  
42 anthropogenic SOA tracers and some POA markers into PMF and resolved seven OA sources in Hong Kong. They found that  
43 45% of OC in Hong Kong during summertime was from secondary formation, and the number could reach up to 65% on  
44 sampling days under regional pollution from the PRD area.

45 All these studies have illustrated the importance of secondary formation to OA in the ambient atmosphere. However, due  
46 to SOA's complex chemical composition and formation mechanisms, a precise prediction of SOA load from individual  
47 precursors at both regional and global scale is still challenging. An SOA tracer based method (TBM) has been developed to  
48 partially solve this problem, which estimates the amount of SOA and SOC formed from the atmospheric oxidation of selected  
49 VOCs (i.e., isoprene, monoterpenes,  $\beta$ -caryophyllene, toluene, and naphthalene) using the mass ratios of tracer-to-SOA/SOC  
50 obtained from laboratory smog chamber experiments (Kleindienst et al., 2007, 2012). However, TBM can only capture SOC  
51 formation from the above-listed VOC precursors, and it may underestimate the actual SOC levels in the ambient atmosphere  
52 due to the lack of SOA tracer-to-SOC ratio values of a broader range of OA precursors. Therefore, besides the SOA tracer  
53 based method, we have also applied PMF to evaluate the contributions of SOC and primary emissions to OA in the region.

54 Many studies have reported the observational evidence of biogenic SOA enhancement induced by anthropogenic emissions,  
55 such as nitrogen oxides ( $\text{NO}_x$ ) and sulfur dioxide ( $\text{SO}_2$ ) (Huang et al., 2014; Xu et al., 2015; Rattanavaraha et al., 2016).  $\text{NO}_x$   
56 is one of the critical drivers of SOA formation through the photochemical oxidation of VOCs via peroxy radical pathways  
57 (Finlayson-Pitts and Pitts, 2000). Nitrogen dioxide ( $\text{NO}_2$ ) reacts with ozone ( $\text{O}_3$ ) to form  $\text{NO}_3$  radical, a critical nighttime gas  
58 oxidant. Several laboratory studies have reported high SOA yields from the oxidation of biogenic VOCs (BVOCs) by  $\text{NO}_3$   
59 radical (Fry et al., 2009; Ng et al., 2008). Some field studies also revealed that SOA formation from  $\text{NO}_3$  oxidation of BVOCs  
60 occurs during both daytime and nighttime (Brown et al., 2013; Rollins et al., 2013). The effect of  $\text{SO}_2$  on SOA formation was  
61 often explained in the context of particle acidity in laboratory studies, which promotes SOA production through acid-catalyzed  
62 heterogeneous reactions (Jang et al., 2002; Surratt et al., 2010). Sulfate was also suggested to enhance isoprene-SOA formation  
63 by acting as the nucleophiles, providing active aerosol surface area, and through the salting-in effect (Rattanavaraha et al.,  
64 2016; Xu et al., 2015). Recently, Wang et al. (2016) proposed a new sulfate formation pathway in aqueous aerosols through  
65  $\text{NO}_2$  oxidation and ammonium neutralization, and synchronous enhancements of both nitrate and SOA production in aqueous  
66 aerosols were reported. These laboratory and field monitoring studies have shown that the abundance and chemical nature of  
67 ambient OA are significantly influenced by the complex interactions among source emissions, anthropogenic activities,  
68 atmospheric physical/chemical processes, and meteorological conditions (An et al., 2019).

69 In this study, we collected 49  $\text{PM}_{2.5}$  samples at an urban site in Hong Kong during a whole year period. Concentration

70 levels of 39 polar organic species were quantified using gas chromatography-mass spectrometry (GC-MS), and their  
71 temporal/meteorological variations were evaluated. With the input of SOA tracers and primary source markers into PMF, we  
72 quantitatively assessed the contributions of various primary and secondary sources to OC. SOC formed from individual  
73 biogenic (i.e., isoprenes, monoterpenes, and  $\beta$ -caryophyllene) and anthropogenic VOCs (i.e., naphthalene) were estimated  
74 using the TBM. Finally, the impacts of anthropogenic pollutants (e.g., NO<sub>2</sub>, O<sub>3</sub>, NO<sub>3</sub>, SO<sub>2</sub>, and tropospheric odd oxygen (O<sub>x</sub>))  
75 and PM<sub>2.5</sub> constituents (e.g., sulfate, acidity, and liquid water content) on total and individual SOCs estimated by both TBM  
76 and PMF were evaluated using Pearson's R analysis and multi-linear regression model. This study provides comprehensive  
77 information on the sources of OA and SOA in Hong Kong as well as direct evidence of anthropogenic influences on the SOA  
78 formation in the region, which may serve as the scientific basis for the formulation of the PM<sub>2.5</sub> mitigation policy in the region.

## 79 2 Method

### 80 2.1. Sample collection

81 The PM<sub>2.5</sub> samples were collected on the 12<sup>th</sup> floor of Science Tower in the Campus of Hong Kong Baptist University  
82 (114°15E, 22°13N, ~40 m above the ground), which is a typical urban site. PM<sub>2.5</sub> samples were collected from September 6,  
83 2011, to August 16, 2012, and a total of 49 samples were collected. A high-volume air sampler was used to collect PM<sub>2.5</sub> onto  
84 a quartz fiber filter (20 cm × 25 cm) at a flow rate of 1.13 m<sup>3</sup> min<sup>-1</sup> for 24 h. The quartz fiber filters were prebaked at 550°C  
85 for 24 h to remove organic contaminants. After sampling, the filters were immediately transferred to the laboratory and stored  
86 at -18°C until analysis.

### 87 2.2. Chemical analysis

88 For EC and OC analysis, a 1 × 1 cm<sup>2</sup> filter was cut and analyzed using a thermal and optical transmittance aerosol carbon  
89 analyzer (Sunset Laboratory, Tigard, OR, USA). Major ions (i.e., Cl<sup>-</sup>, NO<sub>3</sub><sup>-</sup>, SO<sub>4</sub><sup>2-</sup>, C<sub>2</sub>O<sub>4</sub><sup>2-</sup>, Na<sup>+</sup>, Ca<sup>2+</sup>, Mg<sup>2+</sup>, K<sup>+</sup>, NH<sub>4</sub><sup>+</sup>) were  
90 identified and quantified by ion-chromatography (IC, DX500, Dionex, Sunnyvale, CA, USA). Vanadium (V) and Nickel (Ni)  
91 were analyzed using an Agilent 7900 ICP-MS. Detailed analytical methods for the measurements of EC, OC, and ions were  
92 described in our previous work (Hu and Yu, 2013; Ma et al., 2019).

93 Thirty-nine polar organic species were identified and quantified using an Agilent 7890A-5975C GC-MS with prior BSTFA  
94 derivatization (N, O-Bis-(trimethylsilyl)trifluoroacetamide, with 1% trimethylchlorosilane, TMCS). For each aerosol sample,  
95 20 cm<sup>2</sup> of the filter was cut into small pieces and sonicated for 10 min with 10 mL of distilled acetonitrile (HPLC grade); the  
96 extraction was repeated three times. The extracts were combined and filtered through a Millipore 0.45- $\mu$ m PTEE hydrophobic  
97 Teflon filter into a 50 mL round flask, concentrated to ~ 0.5 mL by rotary evaporation, and transferred into a 5 mL reaction  
98 vial. The round flask was rinsed with 1 mL of acetonitrile for three times, and the rinsing solvent was transferred into the

99 reaction vial as well. The final extract was blown to dryness under a gentle stream of pure nitrogen gas at 40 °C and then  
100 derivatized with 100 µL of BSTFA and 50 µL of pyridine at 70 °C for 2 h. After the reaction vial cooled down to room  
101 temperature, 30 µL of tetracosane-d<sub>50</sub> (internal standard, 50 µg mL<sup>-1</sup> in hexane) was added. The derivatives were analyzed by  
102 GC-MS. Two microliters of the derivatized sample or standard were injected and separated on an HP-5MS capillary column  
103 (30.0m×250µm×0.25µm, Agilent J&W). The temperature program and instrument settings were adapted from the method used  
104 by Hu et al. (2008).

105 Saccharides, di- and tricarboxylic acids, 4-nitrocatechol, and cholesterol were identified and quantified using authentic  
106 standards. The SOA tracers were identified using surrogate compounds with similar structures and functional groups (Hu et  
107 al., 2008; Hu and Yu, 2013), and the detailed information was provided in Table 1. Recovery tests of these organic species  
108 were carried out by spiking the mixture of standards onto blank quartz filters, followed by the same sample extraction and  
109 analysis processes. Recoveries of the polar compounds were within the range of 80% to 120%. Analysis of hopanes has been  
110 reported in our previous study (Ma et al., 2019). Four hopanes, including 17 $\alpha$ ,21 $\beta$ -hopane, 17 $\alpha$ ,21 $\beta$ -22R-homhopane,  
111 17 $\alpha$ ,21 $\beta$ -22S-homhopane, and 17 $\alpha$ ,21 $\beta$ -30-norhopane, were measured using an Agilent 6890N-5975 GC-MS with thermal  
112 desorption (TD) method. Recoveries of four hopane standards ranged from 83% to 98%.

### 113 3 Results

114 Hourly meteorological and air quality data (i.e., temperature, relative humidity (RH), O<sub>3</sub>, SO<sub>2</sub>, and NO<sub>2</sub>) in the vicinity of  
115 the sampling site were collected by Hong Kong Environmental Protection Department  
116 (HKEPD) (<http://envf.ust.hk/dataview/gts/current/>). During the sampling period, the ambient temperature ranged from 14.52  
117 to 31.01 °C, with an annual average of 24.17±5.00 °C. The daily average of RH ranged from 52.94% to 97.02%, with a yearly  
118 average of 79.87±10.54%. Heavy rains are common in Hong Kong during summer, which effectively washes out the PM  
119 pollutants.

120 Hong Kong is located at the south-east edge of the Pearl River Delta (PRD) region. PRD is a rapidly developing area with  
121 intensive industrial activities. As described in our previous studies on the analysis of HULIS and water-soluble PM<sub>2.5</sub>-induced  
122 oxidative potential using the same set of PM<sub>2.5</sub> samples (Ma et al., 2019; Cheng et al., 2021) Air pollutants origin from the  
123 northern PRD region can travel together with air masses and transport into Hong Kong. Same as in our previous study (Hu et  
124 al., 2010; Ma et al., 2019), we carefully examined the air mass backward trajectories and the spatial distribution patterns of  
125 SO<sub>2</sub>, the concentration levels of both PM<sub>2.5</sub> and O<sub>3</sub>, and the synoptic weather conditions during the sampling period. We then  
126 categorized all sampling days into three groups, i.e., days mainly influenced by the regional pollution from the PRD region  
127 (regional days), days influenced by long-regional transport of air mass from the northern and eastern China (LRT days), and  
128 days dominated by the locally generated pollutants (local days). The concentration levels of both PM<sub>2.5</sub> and O<sub>3</sub> and the spatial

Formatted: Font: 10 pt, Font color: Auto

Formatted: Font: 10 pt, Font color: Auto

Formatted: Font: 10 pt, Font color: Auto

distribution patterns of SO<sub>2</sub> over the 18 Hong Kong air quality monitoring stations (<http://envf.ust.hk/dataview/gts/current/>) on each sampling day were also checked to assist the classification. A summary of the classification of sampling days and the typical air mass backward-trajectories under the three meteorological categories were presented in Table S2 and Figure S2 in Ma et al. (2019), respectively.

Formatted: Font: 10 pt, Font color: Auto

Formatted: Font: (Default) Times New Roman, 10 pt

Formatted: Font: 10 pt, Font color: Text 1

Formatted: Font: 8 pt, Font color: Text 1

The gas pollutants, i.e., O<sub>3</sub>, NO<sub>2</sub>, O<sub>x</sub>, and SO<sub>2</sub>, showed significantly higher average concentrations on regional days than those on LRT local days (Table 2). The annual mean concentrations of O<sub>3</sub>, NO<sub>2</sub>, and SO<sub>2</sub> were 14.85±8.69 ppb, 37.15±9.76 ppb, and 4.45±2.57 μg m<sup>-3</sup>, respectively. Given that O<sub>3</sub> and NO<sub>2</sub> undergo a rapid photochemical conversion in the ambient atmosphere, the tropospheric odd oxygen O<sub>x</sub> (the sum of O<sub>3</sub> and NO<sub>2</sub>) was calculated as an indicator of atmospheric oxidation capacity. As shown in Table 1, O<sub>x</sub> ranged from 49.72 to 145.90 μg m<sup>-3</sup>, with a mean value of 99.31±27.42 μg m<sup>-3</sup>, indicating a high oxidation capacity of the Hong Kong atmosphere. The annual average concentrations of OC and EC were 4.18±2.37 and 1.02±0.54 μgC m<sup>-3</sup>, respectively. Ambient OC levels observed on regional days (6.15±2.51 μgC m<sup>-3</sup>) were about two times higher than those on LRT and local days; as for EC, it exhibited relative constant levels throughout the year (0.14-2.75 μgC m<sup>-3</sup>). This confirms that EC is mainly emitted locally in Hong Kong, and OC has some regional sources. Moreover, the OC/EC ratios of the collected samples ranged from 1.51 to 10.91, with an annual average value of 4.61, indicating secondary formation could be a dominant source of OA in this region (Mancilla et al., 2015). Our previous study has observed that SOC contributed 45% of OC in Hong Kong during the summer of 2006 (Hu et al., 2010). Here the analysis was expanded to samples taken during the 1-yr period to obtain a more comprehensive understanding of sources and their contributions to ambient OA in Hong Kong, and the factors that impact ambient SOA formation.

### 3.1 Characterization of SOA tracers and other polar oxygenated organic compounds

The concentration levels of 39 organic species, including 14 SOA tracers, 12 saccharides, 11 di- and tricarboxylic acids, 4-nitrocatechol, and cholesterol, under different meteorological conditions, were listed in Table 1.

#### 3.1.1 SOA tracers of isoprene, monoterpenes, β-caryophyllene, and naphthalene

Seven isoprene SOA (Isop<sub>SOA</sub>) tracers, i.e., 2-methylglyceric acid, two methyltetrol isomers (2-methylthreitol and 2-methylerythritol), three C<sub>5</sub>-alkene triol isomers (cis-2-methyl-1,3,4-trihydroxy-1-butene, 3-methyl-2,3,4-trihydroxy-1-butene, and trans-2-methyl-1,3,4-trihydroxy-1-butene), and 3-MeTHF-3,4-diols (including both cis- and trans-3-methyltetrahydrofuran-3,4-diols) were identified and quantified. The sum of all Isop<sub>SOA</sub> tracers ranged from 1.67 to 117.17 ng m<sup>-3</sup>, with the annual mean value of 22.78±26.06 ng m<sup>-3</sup>. Among the Isop<sub>SOA</sub> tracers, methyltetrols and C<sub>5</sub>-alkene triols were the most abundant, and they are suggested to be formed through the acid-catalyzed ring-opening reactions of IEPOX under low-NO<sub>x</sub> condition (Chan et al., 2010; Surratt et al., 2010). Higher concentrations of Isop<sub>SOA</sub> tracers were measured in

158 summer and autumn than in winter and spring. This could be caused by the higher temperature, stronger solar radiation, and  
159 higher emission of isoprene in summer and autumn than in the other two seasons, which promoted the SOA formation from  
160 isoprene. This seasonal pattern is consistent with what were observed in other studies (Ding et al., 2012; Kleindienst et al.,  
161 2007; Lewandowski et al., 2008). However, if we compare the levels of isoprene tracers monitored at different sites during  
162 summer, the total amount of Isop<sub>SOA</sub> tracers measured in Hong Kong was about five times lower than those measured in  
163 several cities in the U.S. and a rural site (WQS site) in the PRD area (Ding et al., 2012; Kleindienst et al., 2007; Lewandowski  
164 et al., 2008). This may be due to the different levels of isoprene, OH radical, and NO<sub>x</sub> at these sampling sites. The 3-MeTHF-  
165 3,4-diols, tracers formed through the intermolecular rearrangement of isoprene epoxydiols (IEPOX) under acidic conditions,  
166 was identified in Hong Kong PM<sub>2.5</sub> samples for the first time. It has an annual mean concentration of 0.23±0.10 ng m<sup>-3</sup>, which  
167 was about 70 times lower than that in Birmingham, U.S. (Rattanavaraha et al., 2016), but was comparable to what was observed  
168 at the WQS site in the PRD area (He et al., 2018). 2-Methylglyceric acid, an isoprene tracer formed from methacrylic acid  
169 epoxide (MAE) and hydroxymethyl-methyl- $\alpha$ -lactone (HMML) under high-NO<sub>x</sub> conditions (Lin et al., 2013; Nguyen et al.,  
170 2015), presented a quite different temporal trend from those of the other six Isop<sub>SOA</sub> tracers, with the highest concentration in  
171 winter, and then autumn, summer, and spring. Chamber studies suggested that MAE is an oxidation product resulting from the  
172 OH addition to methacryloylperoxynitrate (MPAN) and its production is temperature ~~dependant~~dependent (Roberts and  
173 Bertman, 1992; Worton et al., 2013). Under higher temperatures, the loss of MPAN is dominated by thermal decomposition,  
174 which does not produce SOA tracers through the NO/NO<sub>2</sub> pathway. Under lower temperature, thermal decomposition of MPAN  
175 is limited and more MPAN reacts with OH to generate MAE. Therefore, the lower temperatures in winter would favor the  
176 production of MAE and the MAE Isop<sub>SOA</sub> tracers, such as 2-methylglyceric acid. Moreover, all Isop<sub>SOA</sub> tracers exhibited  
177 higher concentrations on regional days than LRT and local days. On regional days, air masses transported from the PRD area  
178 worsened the air quality in Hong Kong, and the higher levels of gaseous pollutants, e.g., O<sub>3</sub>, NO<sub>2</sub>, O<sub>x</sub>, and SO<sub>2</sub> (Table 2),  
179 promoted SOA formation.

180 Generally speaking, at an urban location with anthropogenic NO<sub>x</sub> emissions from automobiles and power plants, the  
181 generation of Isop<sub>SOA</sub> tracers from the MAE NO/NO<sub>2</sub> pathway should be more favored than the HO<sub>2</sub>-IEPOX HO<sub>2</sub> channel.  
182 However, in this study, 94% of the total mass of the quantified Isop<sub>SOA</sub> tracers were produced through the IEPOX HO<sub>2</sub>  
183 pathway. A similar phenomenon was observed at the WQS site in the PRD region (He et al., 2018). Therefore, to better  
184 understand the influences of environmental factors on isoprene SOA formation in the region, we applied the kinetic models  
185 described by Eddingsaas et al. (2010), Worton et al. (2013), and Birdsall et al. (2014) to investigate the fate of both IEPOX  
186 and MAE in the atmosphere. Besides their degradation through acid-catalyzed ring-opening reactions on particles, IEPOX and  
187 MAE can also be oxidized in the gas phase or removed by dry deposition (Eddingsaas et al., 2010). We applied the Kintecus  
188 kinetic model (Ianni, 2015) to quantitatively evaluate the fractions of these two Isop<sub>SOA</sub> intermediates that undergo gas-

189 phase oxidation, aerosol-phase acid-catalyzed ring-opening reaction, and dry deposition processes. Details of the model  
190 calculations were provided in the appendices.

191 Figure 1 showed the comparison of the three elimination processes of IEPOX and MAE during the sampling period in  
192 Hong Kong. Given the high volatility of MAE (vapor pressure:  $9.2 \times 10^{-5}$  atm) (Worton et al., 2013), it has a low tendency to  
193 partition onto the particle phase and its uptake onto aqueous particles is mainly governed by Henry's law constant ( $k_H^{cp}$ ).  
194 Worton et al. (2013) estimated the  $k_H^{cp}$  value of MAE to be  $7.5 \times 10^6$  M atm<sup>-1</sup>, which is 20 times lower than that of IEPOX  
195 ( $1.3 \times 10^8$  M atm<sup>-1</sup>). Moreover, Riedel et al. (2015) suggested that the heterogeneous reactive uptake coefficient of MAE ( $\gamma =$   
196  $4.9 \times 10^{-4}$ ) through the ring-opening reaction was a factor of 30 lower than that of IEPOX. Therefore, as shown in Figure 1,  
197 MAE was primarily eliminated by dry deposition (> 80%) in the gas phase, and only a trivial fraction was degraded through  
198 the ring-opening reactions ( $\leq 2\%$ ). Our results on the fate of MAE were similar to those observed at the University of  
199 California-Blodgett Forest Research Station (UC-BFRS) (Worton et al., 2013). However, our results on the relative  
200 contributions of these three degradation pathways to IEPOX loss were quite different from theirs, indicating a more sensitive  
201 response of IEPOX than MAE to the change of environmental oxidants and conditions. Given the high liquid water content  
202 (LWC; mean:  $57.20 \pm 37.15$   $\mu\text{g m}^{-3}$ ) and particle acidity ( $H_p^+$ ; mean:  $-0.28 \pm 0.42$ ) of  $PM_{2.5}$  samples in this study (Table 2),  
203 particle-phase ring-opening reaction ( $F_{rop}$ ) was the dominant degradation pathway of IEPOX in the Hong Kong atmosphere  
204 (average: 97.6%), and its loss through dry deposition and gas-phase oxidation is almost negligible. The  $F_{rop}$  of IEPOX reported  
205 by Worton et al. (2013) was only 0.02%, mainly due to the much lower LWC (mean:  $0.4$   $\mu\text{g m}^{-3}$ ) and weaker  $H_p^+$  (pH mean:  
206 4.4) of their  $PM_{2.5}$  samples. These results demonstrated that particle-phase LWC and  $H_p^+$  played a more significant role in the  
207 atmospheric degradation of IEPOX than MAE. Results from the kinetic model simulation were strongly supported by the  
208 experimental finding of IEPOX tracers as the dominant Isop<sub>SOA</sub> tracers measured in Hong Kong. The average ratio of IEPOX  
209 tracers to MAE tracers was 16.54 (ranged from 3.00 to 71.58), and the average value of  $F_{rop-IEPOX}/F_{rop-MAE}$  was 191.92,  
210 confirming that the IEPOX HO<sub>2</sub> channel is the major formation pathway of isoprene SOA in the region.

211 Five SOA tracers of monoterpenes (Mono<sub>SOA</sub>), i.e., 3-hydroxyglutaric acid, 3-hydroxy-4,4-dimethylglutaric acid, 3-  
212 methyl-1,2,3-butanetricarboxylic acid, 3-isopropylpentanedioic acid, and 3-acetyl pentanedioic acid, were identified and  
213 quantified. Their summed concentrations ranged from 2.54 to 32.57 ng m<sup>-3</sup>, with an annual average value of  $10.76 \pm 8.04$  ng m<sup>-3</sup>,  
214 comparable to that reported at the WQS site in the PRD region but lower than that measured in the U.S. (Ding et al., 2012;  
215 Kleindienst et al., 2007; Lewandowski et al., 2008). All Mono<sub>SOA</sub> tracers showed the highest level on regional days (mean:  
216  $18.00 \pm 9.28$  ng m<sup>-3</sup>), followed by LRT (mean:  $10.31 \pm 7.33$  ng m<sup>-3</sup>) and local days (mean:  $6.41 \pm 2.75$  ng m<sup>-3</sup>) (Table 1). Although  
217 a higher emission and faster photochemical degradation of monoterpenes are expected in summer due to the intense solar  
218 radiation and high temperature, higher levels of Mono<sub>SOA</sub> tracers were monitored in autumn and winter than in the other two  
219 seasons, similar to what observed at the WQS site (Ding et al., 2014). This seasonal trend of monoterpene SOA tracers may

220 be partly due to the lower mixing height and temperature during autumn/winter, which favored the partition of Mono<sub>SOA</sub>  
221 tracers onto the aerosol phase. Moreover, most of the regional days were identified in autumn and winter. The higher levels of  
222 NO<sub>x</sub>, O<sub>3</sub>, O<sub>x</sub>, and SO<sub>2</sub> on regional days (Table 2) are also responsible for the enhanced monoterpene SOA production in autumn  
223 and winter. Among Mono<sub>SOA</sub> tracers, 3-hydroxyglutaric acid (3HGA) was the most abundant, contributing ~60% of the total  
224 mass of Mono<sub>SOA</sub> tracers. Smog chamber experiments showed that the production yield of 3-methyl-1,2,3-butanetricarboxylic  
225 acid (MBTCA) from α-pinene/NO<sub>x</sub> oxidation was significantly higher than those from the β-pinene/NO<sub>x</sub> and d-limonene/NO<sub>x</sub>  
226 experiments (Jaoui et al., 2005). Therefore, the ratio of 3HGA/MBTCA was used as a criterion to differentiate SOA from α-  
227 pinene and other monoterpenes (Ding et al., 2014). The value of this ratio was obviously higher on regional days (8.58±2.69)  
228 than those on LRT (6.64±3.63) and local days (5.62±3.14), indicating that monoterpenes other than α-pinene, such as β-pinene  
229 and d-limonene, might have a more significant contribution to SOA on regional days in the region.

230 *β*Beta-Caryophyllinic acid is the SOA (Cary<sub>SOA</sub>) tracer of β-caryophyllene, and it ranged from 0.49 to 5.82 ng m<sup>-3</sup>,  
231 with an average annual mean value of 1.53±1.07 ng m<sup>-3</sup>. Similar to the other SOA tracers, β-caryophyllinic acid showed the  
232 highest concentrations on regional days (mean: 2.33±1.21 ng m<sup>-3</sup>) than LRT (1.73±1.16 ng m<sup>-3</sup>) and local days (0.94±0.41 ng  
233 m<sup>-3</sup>) (Table 1). For its seasonal trend, β-caryophyllinic acid also exhibited the highest concentration in autumn and winter than  
234 the other two seasons. The SOA tracer of toluene, 2,3-dihydroxy-4-oxopentanoid acid, was undetectable in this study, mainly  
235 due to its trace level in the Hong Kong atmosphere (Hu et al., 2008) and the limited sensitivity of GC-quadruple MS. Even in  
236 our previous study on a batch of summer PM<sub>2.5</sub> samples using a more sensitive GC-ion trap MS, it was barely quantified with  
237 a concentration of less than 1 ng m<sup>-3</sup> in most samples (Hu et al., 2008). Phthalic acid was suggested as the SOA tracer of  
238 naphthalene, given its abundance in both naphthalene-SOA and ambient OA (Kleindienst et al., 2012). With the awareness of  
239 the potential uncertainties, e.g., the primary origin of phthalic acid from biomass burning, we adopted phthalic acid as the SOA  
240 tracer of naphthalene representing the SOA formation from anthropogenic VOCs. The concentration levels of phthalic acid  
241 ranged from 0.80 to 16.42 ng m<sup>-3</sup>, with an average of 4.31±3.39 ng m<sup>-3</sup>. Similar to the other SOA tracers, it also showed the  
242 highest concentrations on regional days (7.16±3.61 ng m<sup>-3</sup>) than LRT (4.97±3.30 ng m<sup>-3</sup>) and local days (2.26±1.38 ng m<sup>-3</sup>)  
243 (Table 1).

### 244 3.1.2 Saccharides and dicarboxylic acids

245 Twelve saccharides, i.e., levoglucosan, arabitol, fructose, meso-erythritol, sucrose, galactosan, mannitol, sorbitol,  
246 galactose, glucose, xylose, and xylitol, have been quantified. Of the 12 saccharides, levoglucosan, the tracer of BB, was by far  
247 the most abundant (range: 0.64-474.15 ng m<sup>-3</sup>; mean: 75.02±111.43 ng m<sup>-3</sup>). It showed the highest levels on regional days  
248 (about 6 times higher than that on local days), especially during winter when BB activities in the PRD region were most  
249 frequent. Two primary saccharides, i.e., fructose and xylose, also exhibited the highest levels on regional days. They showed

Formatted: Font: Italic

250 good correlations with levoglucosan ( $R^2=0.65$  and  $0.93$ ), suggesting that they could be from BB as well.

251 Among the identified dicarboxylic acids, oxalic acid was the most abundant, followed by terephthalic acid, phthalic acid,  
252 malic acid, succinic acid, and others. Most dicarboxylic acids, including the five most abundant ones, showed higher levels on  
253 regional days; they were found with higher levels in winter and autumn as well. This temporal trend is similar to what we have  
254 observed for Mono<sub>SOA</sub> tracers and most saccharides, indicating that regional pollution had a dominant influence on the  
255 abundance of both primary and secondary aerosols in Hong Kong, far exceeding the influence of other environmental  
256 parameters, such as temperature and solar radiation. Atmospheric dicarboxylic acids have various sources. For example, oxalic  
257 acid was suggested to be secondarily formed from biogenic emissions and anthropogenic sources (e.g., BB and automobile  
258 exhaust) through both gas-phase reactions and in-cloud processing (Yu et al., 2005). Malic acid was suggested to be the photo-  
259 degradation product of both succinic acid and biogenic SOA compounds (Hu and Yu, 2013). In this study, malic acid was  
260 found to be strongly correlated with 3HGA ( $R^2=0.96$ ) and  $\Sigma$ Mono<sub>SOA</sub> tracers ( $R^2=0.95$ ) throughout the year, providing more  
261 evidence to the hypothesis that malic acid is a late-stage oxidation product of BVOCs, especially monoterpenes (Hu and Yu,  
262 2013). Ambient terephthalic acid was mainly directly emitted from plastic wastes incineration (Simoneit et al., 2005) and was  
263 used as a marker of waste incineration.

264 Besides dicarboxylic acids, two benzenetricarboxylic acids (i.e., 1,2,3- and 1,2,4-benzenetricarboxylic acids), 4-  
265 nitrocatechol, and cholesterol were also quantified. The two benzenetricarboxylic acids were suggested to be the photo-  
266 degradation products of polycyclic aromatic hydrocarbons (PAHs) emitted from the combustion activities (Kautzman et al.,  
267 2010). We have previously identified them in the water-soluble humic-like substances (HULIS) extracts of PM<sub>2.5</sub> samples  
268 collected in Beijing and Hong Kong (Ma et al., 2018, 2019). The annual mean concentrations of 1,2,3- and 1,2,4-  
269 benzenetricarboxylic acids measured in this study were  $2.27\pm 1.97$  ng m<sup>-3</sup> (range: 0.47-9.50 ng m<sup>-3</sup>) and  $3.13\pm 2.68$  ng m<sup>-3</sup> (0.47-  
270 12.54 ng m<sup>-3</sup>), respectively, which were comparable to what measured at the other four sites in the PRD region (He et al., 2018).  
271 The 4-nitrocatechol, which was secondarily generated from the photo-oxidation of naphthalene, was suggested as the tracer of  
272 atmospheric aging of BB plume (Kitanovski et al., 2012). It strongly correlated with levoglucosan ( $R^2=0.88$ ) and exhibited  
273 higher levels on regional days and during winter, which further confirmed its BB origin in the region. Therefore, the two  
274 benzenetricarboxylic acids and 4-nitrocatechol were included in PMF analysis as the SOA tracers of BB aging.

### 275 3.2 Source apportionment of organic aerosols

276 In this study, [the US EPA PMF 5.0 analysis](#) was ~~performed~~ used to determine the major OA sources and quantify their  
277 contributions to OC. Eighteen species were input into PMF, including EC, OC, Ni, V, major ions, and various primary and  
278 secondary organic tracers. Given their similar origins, some organic tracers were lumped together, and the lumped species  
279 were used as the fitting species in PMF. They were (1) C<sub>5</sub>-alkene triols, sum of the three C<sub>5</sub>-alkene triols isomers; (2) IsopT,

280 the sum of two methyltetrol isomers and 2-methyl glyceric acid; (3) MonoT, the sum of the five monoterpenes SOA tracers;  
281 and (4) Hopane, the sum of the four hopanes. Since C<sub>5</sub>-alkene triols were not in the SOA tracers list of the TBM (Kleindienst  
282 et al., 2007), the lumped C<sub>5</sub>-alkene triols were used as a separated fitting species in PMF. PMF solutions were tested with 4 to  
283 8 factors. A hundred base runs were performed in each modeling run, and the run with the minimum Q value was selected. The  
284 uncertainty values of each input species were calculated using the method described in our previous studies (Hu et al., 2010;  
285 Ma et al., 2016), which were set to be 20% of the mean concentrations for OC and EC, and 40% of mean values for cations,  
286 anions, and all organic species. An extra modeling uncertainty of 10% was used to account for possible temporal changes in  
287 the source profiles. The Q<sub>Robust</sub>/Q<sub>True</sub> ratio was 1.00, and scaled residuals were normally distributed between -0.2 and 0.2,  
288 indicating no influence of outliers on the solution. A hundred bootstrap runs were performed with a minimum correlation R-  
289 value to examine the base run solution's stability and uncertainty. All bootstrapped factors were explicitly mapped to factors  
290 resolved in base solution with no exception. In the displacement (DISP) assessment, no error was found, and the drop of Q  
291 value was less than 1%, suggesting a stable solution. No swap factor appeared at dQ<sub>max</sub>=4, indicating there was no considerable  
292 rotational ambiguity in the solution. Rotations were introduced to the solutions by adjusting the FPEAK value from -1 to +1,  
293 and the non-rotated solutions (FPEAK=0.0) were considered to be the most interpretable ones. Moreover, a strong linear  
294 correlation between the measured and PMF-predicted OC (OC<sub>PMF</sub>) (R<sup>2</sup>=0.92) was observed, which also suggested a reliable  
295 PMF solution. ~~Moreover, a strong linear correlation between the measured and PMF-predicted OC (OC<sub>PMF</sub>) (R<sup>2</sup>=0.92) was  
296 observed, which also suggested a reliable PMF solution.~~

297 As shown in Figure 2, the first factor was distinguished by high loadings of oxalate and biogenic SOA tracers, suggesting  
298 the secondary origin of this source. The second factor was dominated by large amounts of SO<sub>4</sub><sup>2-</sup> and NH<sub>4</sub><sup>+</sup>, suggesting the  
299 process of secondary sulfate formation. In the third factor, about 90% of levoglucosan was resolved into it, accompanied by  
300 4-nitrocatechol, phthalic acid, and the two benzenetricarboxylic acids, indicating both the primary emission and aging of BB  
301 plume. Therefore, this factor was defined as BB and SOA (BB/SOA). The fourth factor was identified as vehicular emissions  
302 due to the large amounts of hopanes and EC resolved. The fifth factor has large amounts of Ni and V, which are signatures of  
303 residual oil combustion from the marine vessel (Viana et al., 2009). It is well known that Hong Kong is one of the busiest  
304 container ports globally, which handles 50% of the PRD's total cargo throughput. Therefore, the fifth factor was identified as  
305 marine vessels. The sixth factor has a high loading of Na<sup>+</sup>, Mg<sup>2+</sup>, and Ca<sup>2+</sup>, indicating the sea salt source.

306 ~~The amount of OC apportioned to each factor in PMF analysis was considered as the contribution of that source to ambient~~  
307 ~~OC. Therefore, the two leading sources contributing to ambient OC in Hong Kong were BB (including both primary emission~~  
308 ~~and aging process, OC<sub>BB</sub>: 27.9%, 1.17±1.99 μgC m<sup>-3</sup>) and SOA (SOC<sub>SOA</sub>: 27.5%, 1.15±0.82 μgC m<sup>-3</sup>), followed by marine~~  
309 ~~vessels (OC<sub>marine</sub>: 15.6%, 0.65±0.58 μgC m<sup>-3</sup>), SS (SOC<sub>SS</sub>: 14.5%, 0.60±0.46 μgC m<sup>-3</sup>), vehicle emissions (OC<sub>vehicle</sub>: 10.5%,~~  
310 ~~0.44±0.42 μgC m<sup>-3</sup>), and sea salt (OC<sub>sea</sub>: 4.0%, 0.17±0.19 μgC m<sup>-3</sup>) (Table 2 and Fig. 3). Since a fraction of SOA from the~~

Formatted: Font: 10 pt, Font color: Auto

aging of BB (SOC<sub>BB</sub>) was resolved into the BB/SOA factor-, we calculated SOC<sub>BB</sub> using the following equation:

$$\text{SOC}_{\text{BB}} = \text{OC}_{\text{BB}} - \frac{[\text{LEVO}_{\text{BB}}]}{0.082} \quad (1)$$

where OC<sub>BB</sub> and [LEVO<sub>BB</sub>] are the amounts of OC and levoglucosan resolved in the BB/SOA factor. Using levoglucosan as the tracer of primarily emitted BB OA, we calculated the amounts of POC from BB (POC<sub>BB</sub>) by dividing [LEVO]<sub>BB</sub> with 0.082, where 0.082 is the average ratio of levoglucosan to POC from the burning of major types of Chinese cereal straws (i.e., rice, wheat, and corn) obtained in the combustion chamber experiments (Zhang et al., 2007). As cereal straws are one of the most common BB fuels in China, the above ratio (0.082) has been used to estimate BB contribution to POC in both Beijing (Zhang et al., 2008) and Hong Kong (Sang et al., 2011). Therefore, it was adopted to calculate POC<sub>BB</sub> in this study.

Based on PMF results, the source-specific contributions to OC were presented in Table 2 and demonstrated in Fig. 3. The total SOC apportioned by PMF (SOC<sub>PMF</sub>), i.e., the sum of SOC<sub>SOA</sub>, SOC<sub>SS</sub>, and SOC<sub>BB</sub>, accounted for 51.4% (2.15±1.37 μgC m<sup>-3</sup>) of OC in Hong Kong, with the secondary organic-rich sources (i.e., SOC<sub>SOA</sub>+SOC<sub>BB</sub>) contributing 36.9% (1.54±1.13 μgC m<sup>-3</sup>) of total OC. Huang et al. (2014) also reported that secondary organic-rich sources accounted for 30-40% of OC in Guangzhou, another PRD site. A higher level of SOC<sub>PMF</sub> and its contribution to OC were observed on regional days (3.27±1.18 μgC m<sup>-3</sup>, 57.4%) than on LRT (2.36±1.54 μgC m<sup>-3</sup>, 53.0%) and local days (1.36±0.81 μgC m<sup>-3</sup>, 43.6%). An even starker difference in the amounts of SOC<sub>BB</sub> between regional and local days was observed, which was eight times higher on the regional days. This suggested that non-local sources were the dominant contributors to SOC<sub>BB</sub>. BB activities were intensive in the PRD region, especially during fall and winter. On regional days, freshly emitted and aged gaseous and aerosol phase pollutants from the open burning of rice straws and other crops were transported from the northern PRD region into Hong Kong (Hu et al., 2010). Huang et al. (2014) examined the aging of BB plume at low temperatures. They found that the production of BB SOA was rapid at a typical OH radical concentration of wintertime China, and the amount of BB SOA may exceed BB POA in 4-14 h even at -10 °C. Given that the average temperature in Hong Kong during autumn and winter was 26.15 °C and 17.76 °C, the formation of BB SOA should be even fastly achieved during the regional transport. As expected, SOC<sub>SOA</sub> also showed a higher average concentration on regional days (1.75±0.75 μgC m<sup>-3</sup>) than on LRT (1.14±0.82 μgC m<sup>-3</sup>) and local days (0.78±0.65 μgC m<sup>-3</sup>), which is consistent with the trends of all SOA tracers. Although SOC from secondary inorganic-rich source (SOC<sub>SS</sub>) exhibited the highest levels (0.82±0.38 μgC m<sup>-3</sup>) on regional days as well, its contribution to OC was relatively stable under the three synoptic conditions (Fig. 3). Several studies showed that SO<sub>2</sub> transported from the northern PRD region promoted secondary sulfate formation in Hong Kong through both gas-phase and in-cloud oxidation pathways (Lu and Fung, 2016; Yu et al., 2005; Yuan et al., 2006). A recent study proposed that the sulfate formation in aqueous aerosols through NO<sub>2</sub> oxidation and ammonium neutralization can simultaneously enhance the production of both nitrate and SOA (Wang et al., 2016), which helps explain the considerable amount of SOC<sub>SS</sub> apportioned.

OC from the four primary sources, i.e., POC<sub>BB</sub>, OC<sub>marine</sub>, OC<sub>vehicle</sub>, and OC<sub>sea</sub>, accounted for 48.6% of total OC throughout

342 the year. Similar to  $\text{SOC}_{\text{BB}}$ ,  $\text{POC}_{\text{BB}}$  showed a higher level ( $1.38 \pm 1.75 \mu\text{gC m}^{-3}$ ) on regional days due to a large number of  
343 emissions from BB activities in the northern PRD area.  $\text{OC}_{\text{vehicle}}$  remained a higher contribution on local days (15.6%,  
344  $0.49 \pm 0.46 \mu\text{gC m}^{-3}$ ), consistent with our previous finding that vehicle emission is a local pollution source (Hu et al., 2010).  
345 Similarly, marine vessels accounted for a greater amount and larger fraction of OC on local days (32.0%,  $1.00 \pm 0.63 \mu\text{gC m}^{-3}$ )  
346 than LRT (5.2%,  $0.23 \pm 0.19 \mu\text{gC m}^{-3}$ ) and regional days (6.5%,  $0.37 \pm 0.21 \mu\text{gC m}^{-3}$ ). On local days, the southeastern to  
347 southwestern wind brought pollutants from residual oil combustion from the ocean into Hong Kong, leading to a higher  
348  $\text{OC}_{\text{marine}}$ .

349 In summary, both secondary aerosol sources and air mass origins play important roles in atmospheric OC in Hong Kong.  
350 On regional days, air mass transported from the northern PRD area brought large amounts of air pollutants into Hong Kong,  
351 which promoted the SOA production from both anthropogenic emissions and BVOCs and resulted in a fraction of 57.4% of  
352 OC being secondarily formed. On the other hand, local sources, including vehicle emissions and marine vessels, became more  
353 critical and significantly contributed to OC (56.4%) on local days.

### 354 3.3 Estimation of SOC origin

355 To better understand the SOA precursors and their contributions to SOA/SOC in the region, we adopted a tracer-based  
356 method (Kleindienst et al., 2007, 2012; Offenberg et al., 2007) to estimate the SOA/SOC formation from a group of selected  
357 biogenic and anthropogenic hydrocarbons, i.e., isoprene, monoterpenes,  $\beta$ -caryophyllene, and naphthalene. The mass ratio of  
358 tracer compounds to the total SOC ( $f_{\text{SOC}}$ ) generated from individual VOC precursors was derived from smog chamber  
359 experiments (Kleindienst et al., 2007; Offenberg et al., 2007). By assuming the same  $f_{\text{SOC}}$  value of the precursor under smog  
360 chamber conditions and in ambient air, one can use the quantified SOA tracer concentrations to estimate the amount of SOC  
361 from that precursor in the real atmosphere. It has been well noted that results obtained from this tracer-based method are subject  
362 to potential uncertainties from various aspects, e.g., the larger variation of precursor concentrations and more complicated  
363 environmental conditions in the real atmosphere than in smog chamber experiments, the decay of some tracer compounds  
364 during transport, mismatch of ambient and smog chamber generated SOA compositions, using surrogates other than ketopinic  
365 acid for the quantification of tracer compounds, and so on (Ding et al., 2014; Hu et al., 2008; Kleindienst et al., 2012, 2007).  
366 However, using the tracer-based method, we can at least have a rough estimation of the key SOA precursors in the region,  
367 their contributions to ambient OC, and the amount of SOC from unknown precursors. Wang et al. (2013) noted that the SOA  
368 tracer-based method would significantly underestimate  $\text{SOC}_{\text{Mono}}$  in the PRD region. Ding et al. (2014) gave a reasonable  
369 explanation that the mismatch of monoterpene tracers measured in ambient air and used to derive  $f_{\text{SOC}}$  of monoterpenes in  
370 chamber studies may increase the uncertainty of  $\text{SOC}_{\text{Mono}}$ . Thus they picked the five  $\text{Mono}_{\text{SOA}}$  tracers measured in their  
371 samples and derived the  $f_{\text{SOC}}$  and  $f_{\text{SOA}}$  values using the SOA tracers data and SOA/SOC concentrations reported by Offenberg

372 et al. (2007). In this study, we only measured five out of nine monoterpene SOA tracers in Offenberg et al.'s (2007) study.  
373 Similar to Ding et al. (2014), to lower the uncertainty induced from the mismatch of SOA tracer compositions, we derived a  
374  $f_{\text{SOC\_mono}}$  value of 0.047 based on Offenberg et al.'s experimental data (2007) and applied it to estimate  $\text{SOC\_Mono}$ . Many  
375 research groups have adopted this tracer-based method to assess SOC productions from the five studied VOCs at various  
376 locations in the world, and reasonable results have been obtained (Ding et al., 2012; Fu et al., 2014; Hu et al., 2008; Hu and  
377 Yu, 2013; Kleindienst et al., 2012, 2007; Lewandowski et al., 2008).

378 As shown in Table 2, SOC estimated by the tracer-based method ( $\text{SOC}_{\text{TBM}}$ ) ranged from 0.11 to 1.53  $\mu\text{gC m}^{-3}$  in Hong  
379 Kong, accounting for 3.8% to 22.7% of ambient OC levels. It exhibited the same trend as OC and  $\text{SOC}_{\text{PMF}}$ , i.e., with higher  
380 concentrations on regional days ( $0.81 \pm 0.35 \mu\text{gC m}^{-3}$ ) than on LRT ( $0.50 \pm 0.29 \mu\text{gC m}^{-3}$ ) and local days ( $0.28 \pm 0.13 \mu\text{gC m}^{-3}$ ).  
381 Similar to our previous study, monoterpenes were found to be the most significant SOC contributor in the region, with  
382  $\text{SOC\_Mono}$  ranging from 0.05 to 0.69  $\mu\text{gC m}^{-3}$  and having an average concentration of  $0.23 \pm 0.17 \mu\text{gC m}^{-3}$ .  $\text{SOC\_Iso}$  and  $\text{SOC\_Cary}$ ,  
383 on the other hand, were about three times smaller than  $\text{SOC\_Mono}$  and were  $0.08 \pm 0.09 \mu\text{gC m}^{-3}$  and  $0.07 \pm 0.05 \mu\text{gC m}^{-3}$ ,  
384 respectively. Smog chamber experiments have been carried out to study the SOA yields from  $\cdot\text{OH}$  oxidation, ozonolysis, and  
385 nitrate radical ( $\text{NO}_3$ ) oxidation of monoterpenes and isoprene, and monoterpenes were found to be more effective in SOA  
386 production than isoprene (Lee et al., 2006a, 2006b). Highly oxygenated organic molecules with low and extremely low  
387 volatility were formed from the oxidation of monoterpenes and observed in both laboratory experiments and field  
388 measurements (Ehn et al., 2014; Jokinen et al., 2015; Zhang et al., 2018). Moreover, a synergistic  $\text{O}_3 + \text{OH}$  oxidation pathway  
389 of monoterpenes was recently proposed, which leads to the formation of extremely low-volatility oligomers and may result in  
390 even larger monoterpene SOA yields in the real atmosphere than what observed in the smog chamber experiments (Kenseth et  
391 al., 2018). Tsui et al. (2009) reported a total BVOC emission of  $8.6 \times 10^9 \text{ gC yr}^{-1}$  in Hong Kong, with 40% from monoterpenes  
392 and 30% from isoprene. The remaining 30% could be sesquiterpenes (e.g.,  $\beta$ -caryophyllene) or other BVOCs. Therefore, the  
393 predominance of monoterpenes SOA in BVOCs-derived SOC is likely due to the combined effects of their high SOA yields  
394 and large emissions in the region. Like the SOA tracers, SOC from the four precursors all showed the highest level on regional  
395 days than those on LRT and local days (Table 2). On regional days, large amounts of VOC precursors and gaseous oxidants  
396 could be brought into Hong Kong through the regional transport of air masses from northern PRD and oxidized along the way.  
397 Conversely, on local days, the ocean breeze brings clean air masses from the South China Sea into Hong Kong, leading to a  
398 dilution effect of local air pollution. These results highlight that air mass origins play an important role in the SOC formation  
399 from both biogenic and anthropogenic VOCs. Given that  $\text{SOC}_{\text{TBM}}$  is calculated based on the concentration levels of individual  
400 SOA tracers measured in the ambient aerosols, it is reasonable that SOC attributed to each VOC precursor showed the same  
401 meteorological variations as their SOA tracers.

402 We observed similar temporal trends between  $\text{SOC}_{\text{PMF}}$  and  $\text{SOC}_{\text{TBM}}$  ( $R^2=0.71$ ). However,  $\text{SOC}_{\text{TBM}}$  only accounted for

26.5% of  $\text{SOC}_{\text{PMF}}$ , suggesting SOC must have been underestimated by the tracer-based method. A reasonable explanation is that secondary formation from nighttime reactions, multi-phase reactions, and other SOA precursors are not considered in the SOA tracer-based method. ~~Because P~~ parameters used in the tracer-based method were derived from pure gas-phase photo-oxidation of VOC precursors in smog chambers (Kleindienst et al., 2007, 2009). Therefore, it is better to be used as a complementary method with PMF in the source apportionment study of ambient OC, especially SOC.

### 3.4 Effects of anthropogenic influences on secondary aerosol formation

Increasing evidence from laboratory studies and ambient observations has shown that anthropogenic emissions can significantly affect SOA formation from terpenoids through multiple chemical processes in both daytime and nighttime (Xu et al., 2013; Zhang et al., 2018). We conducted the Pearson's R correlation analysis of all SOC terms (i.e.,  $\text{SOC}_{\text{Iso}}$ ,  $\text{SOC}_{\text{Mono}}$ ,  $\text{SOC}_{\text{Cary}}$ ,  $\text{SOC}_{\text{Nap}}$ ,  $\text{SOC}_{\text{TBM}}$ ,  $\text{SOC}_{\text{PMF}}$ ,  $\text{SOC}_{\text{BB}}$ ,  $\text{SOC}_{\text{SOA}}$ , and  $\text{SOC}_{\text{SS}}$ ) with  $\text{O}_3$ ,  $\text{NO}_2$ ,  $\text{SO}_2$ ,  $\text{O}_\text{X}$ ,  $\text{NO}_3$ , sulfate, particle acidity ( $\text{H}_\text{p}^+$ ), and particle liquid water content ( $\text{LWC}_\text{p}$ ) (Table 3). Details on the calculation of  $\text{H}_\text{p}^+$  and  $\text{LWC}_\text{p}$  were presented in Appendix B. Since  $\text{NO}_3$  was not directly monitored at HKEPD stations, its mixing ratio was estimated using the following equation:

$$[\text{NO}_3] = \frac{k_1[\text{O}_3][\text{NO}_2]}{\sum k_i[\text{VOC}_i]} \quad (2)$$

The numerator is the production of  $\text{NO}_3$  ( $\text{p}[\text{NO}_3]$ ) from  $\text{O}_3$  and  $\text{NO}_2$ , and the denominator is the reactivity of  $\text{NO}_3$  for  $\text{NO}_3$ -VOCs reactions. From the IUPAC database, we obtained the temperature-dependent expression of  $k_1$  ( $\text{cm}^3 \text{ molecules}^{-1} \text{ s}^{-1}$ ), the production rate constant of  $\text{NO}_3$  as  $1.4 \times 10^{-13} \text{ E-13 exp EXP}(-2470/T)$ , where T is the ambient temperature in Kelvin. Therefore, using  $k_1$  and the measured concentration levels of  $[\text{O}_3]$  and  $[\text{NO}_2]$ , we calculated  $\text{p}[\text{NO}_3]$  (Table 2). Brown et al. (2016) reported a  $\text{NO}_3$ -VOCs reactivity of  $6.5 \pm 6.8 \times 10^{-3} \text{ s}^{-1}$  in Hong Kong with a corresponding  $\text{NO}_3$  lifetime of 2.5 min.  $\text{NO}_3$  was then calculated as the ratio of  $\text{p}[\text{NO}_3]$  to this  $\text{NO}_3$  reactivity value, and an annual mean level of  $70 \pm 47$  ppt was estimated.

As we mentioned earlier,  $\text{O}_\text{X}$  is an indicator of atmospheric oxidation capacity. Five SOC terms, i.e.,  $\text{SOC}_{\text{Mono}}$ ,  $\text{SOC}_{\text{Nap}}$ ,  $\text{SOC}_{\text{TBM}}$ ,  $\text{SOC}_{\text{SOA}}$ , and  $\text{SOC}_{\text{PMF}}$ , showed significant positive correlations with  $\text{O}_\text{X}$ , especially  $\text{SOC}_{\text{SOA}}$  and  $\text{SOC}_{\text{PMF}}$  ( $R > 0.7$ ,  $P < 0.01$ ). However, only  $\text{SOC}_{\text{SOA}}$  and  $\text{SOC}_{\text{SS}}$  were found to be significantly correlated with  $\text{O}_3$  ( $R > 0.50$ ,  $P < 0.01$ ). As for  $\text{NO}_2$ , another critical component of  $\text{O}_\text{X}$ , it exhibited statistically significant positive correlations with not only  $\text{SOC}_{\text{SOA}}$  and  $\text{SOC}_{\text{PMF}}$ , but also several TBM estimated SOCs, including  $\text{SOC}_{\text{TBM}}$ ,  $\text{SOC}_{\text{Mono}}$ ,  $\text{SOC}_{\text{Nap}}$ , and  $\text{SOC}_{\text{Cary}}$ . This may be because SOA tracers used in TBM were produced from the photo-oxidation of these VOC precursors in the presence of  $\text{NO}_\text{X}$  (Kleindienst et al., 2007). The significant positive correlations between  $\text{NO}_2$  and  $\text{SOC}_{\text{SOA}}$  and  $\text{SOC}_{\text{PMF}}$  also suggests that the daytime oxidation processes involving  $\text{NO}_\text{X}$  are critical SOA formation pathways in the region. Significant correlations with  $R > 0.5$  between  $\text{NO}_3$  and  $\text{SOC}_{\text{Mono}}$ ,  $\text{SOC}_{\text{SOA}}$ ,  $\text{SOC}_{\text{PMF}}$ , and  $\text{SOC}_{\text{SS}}$  were also observed. BVOCs were found to account for  $> 80\%$  of the  $\text{NO}_3$  reactivity in Hong Kong (Brown et al., 2016), with monoterpenes as the leading contributor. Both Zhang et al. (2018) and Xu et al. (2013) have reported an enhancement of nighttime monoterpenes SOA in the southeastern U.S. by  $\text{NO}_3$ -monoterpenes reactions.

433 Therefore, our findings indicate that SOA formation through nighttime NO<sub>3</sub> oxidation of biogenic VOCs, especially  
434 monoterpenes, may have made a considerable contribution to the SOA loading in Hong Kong. However, more field  
435 measurement data, e.g., quantification of the particle-phase organic nitrates using real-time online mass spectrometry  
436 techniques, are needed to examine the impact of NO<sub>x</sub> processing on SOA formation in the region.

437 Since NO<sub>3</sub> is a key precursor of nighttime production of HNO<sub>3</sub>, and nitrate is a significant component of secondary inorganic  
438 aerosols, it rationalized the correlations between NO<sub>3</sub> and SOC<sub>SS</sub>. Six SOC terms, i.e., SOC<sub>Mono</sub>, SOC<sub>Nap</sub>, SOC<sub>TBM</sub>, SOC<sub>SOA</sub>,  
439 SOC<sub>SS</sub>, and SOC<sub>PMF</sub>, showed significant positive correlations with sulfate, especially SOC<sub>SS</sub> and SOC<sub>PMF</sub> (R≥0.8, P<0.01).  
440 Given that sulfate is the key component of secondary inorganic aerosol, such a strong correlation between SOC<sub>SS</sub> and sulfate  
441 is expected. Moreover, several studies have suggested that sulfate also plays a dominant role in the production of aerosol-phase  
442 organosulfates through both nucleophilic addition reactions and the salting-in effect (Lin et al., 2012; Riva et al., 2015; Xu et  
443 al., 2015).

444 We then performed multivariate linear regression (MLR) analysis to obtain a quantitative and comprehensive understanding  
445 of the impacts of gaseous oxidants and aerosol characteristics on SOC<sub>TBM</sub>, SOC<sub>PMF</sub>, and the individual PMF resolved SOC<sub>s</sub>  
446 (i.e., SOC<sub>SS</sub>, SOC<sub>SOA</sub>, and SOC<sub>BB</sub>). Six parameters, namely O<sub>3</sub>, NO<sub>2</sub>, NO<sub>3</sub>, sulfate, H<sub>p</sub><sup>+</sup>, and LWC<sub>p</sub>, were included in the  
447 preliminary runs. However, the MLR results showed that O<sub>3</sub> was an insignificant factor for all SOC terms, even with negative  
448 regression coefficients. Pearson's R analysis also showed that SOC was more NO<sub>2</sub> dependent than O<sub>3</sub>. Therefore, it was  
449 excluded from the final MLR analysis, and the results were shown in Table 4.

450 We found that ~~three-two~~ parameters, i.e., ~~NO<sub>2</sub>~~-sulfate, and NO<sub>3</sub>, have statistically significant positive linear relationships  
451 (P ≤ 0.001) with SOC<sub>SS</sub>, and the regression coefficients were ~~0.303~~, 0.913, and 0.234, respectively. The result is reasonable  
452 and consistent with what was observed from ~~the~~ Pearson's R analysis, given that sulfate is the critical component in the PMF  
453 resolved SS factor, and ~~both NO<sub>2</sub> and NO<sub>3</sub> are~~ is the precursors of nitrate through HNO<sub>3</sub> formation at nighttime. As for SOC<sub>BB</sub>,  
454 three parameters, i.e., NO<sub>2</sub>, NO<sub>3</sub>, and H<sub>p</sub><sup>+</sup>, showed significant ~~positive~~-linear relationships with it (P<0.01), with a regression  
455 coefficient of 0.639, ~~-0.509~~, and 0.503, respectively. This indicates that a 1 mol L<sup>-1</sup> increase in particle acidity was associated  
456 with a 0.503 μgC m<sup>-3</sup> increase in SOC from BB aging. Phenols, which are produced from the combustion of lignin, are a typical  
457 class of gaseous compounds emitted in large amounts from BB (Bruns et al., 2016; Schauer et al., 2001). Recent laboratory  
458 studies indicate that phenols can undergo multi-phase photochemical reactions in the atmosphere with the formation of  
459 nitrophenols and nitrocatechols (Finewax et al., 2018; Yu et al., 2014). Vione et al. (2001) observed the aqueous phase  
460 photonitration of phenols, which was pH-dependent with more nitro-compounds generated at lower pH. Given the strong  
461 particle acidity (pH annual mean: -0.28) observed in the Hong Kong atmosphere, the formation of the 4-nitrocatechol and its  
462 analogs may be favored in the BB plume, which enhances SOC<sub>BB</sub> formation.

463 Both sulfate and NO<sub>2</sub> were found as the statistically significant factors that positively correlated with SOC<sub>PMF</sub>, with

464 regression coefficients of 0.530 and 0.373, respectively ( $P < 0.001$ , Table 4). This suggests reducing the sulfate level by 1  $\mu\text{g}$   
465  $\text{m}^{-3}$  and  $\text{NO}_2$  level by 1 ppb could lower the total PMF-apportioned SOC by 0.530 and 0.373  $\mu\text{gC m}^{-3}$ , respectively.  $\text{NO}_2$  was  
466 also the most significant factor influencing  $\text{SOC}_{\text{TBM}}$ , with a regression coefficient of 0.383 ( $P < 0.001$ ), indicating that a decrease  
467 of  $\text{NO}_2$  by 1 ppb can reduce  $\text{SOC}_{\text{TBM}}$  by 0.383  $\mu\text{gC m}^{-3}$ . As for  $\text{SOC}_{\text{SOA}}$ , we found  $\text{NO}_3$  as the most significant parameter  
468 ( $P < 0.01$ ), and a decrease of 1 ppb  $\text{NO}_3$  can lead to a reduction of  $\text{SOC}_{\text{SOA}}$  by 0.384  $\mu\text{gC m}^{-3}$  when holding other covariates  
469 unchanged. These results are consistent with what was observed from the Pearson's R analysis, indicating the importance of  
470  $\text{NO}_x$  processing on both daytime and nighttime SOA production in the region.

#### 471 4 Conclusions

472 In this study, we identified and quantitatively assessed the contributions of six primary and secondary sources to ambient  
473 OC in Hong Kong, and secondary formation was found to be the leading contributor. Anthropogenic emissions, including  $\text{NO}_2$ ,  
474  $\text{O}_x$ ,  $\text{NO}_3$ , and sulfate, significantly influenced SOA formation in the region. In particular,  $\text{NO}_x$  processing in both daytime and  
475 nighttime has played a critical role. Although the ambient  $\text{NO}_2$  level has dropped by 33.3% from 1999 to 2019 (the government  
476 of HKSAR, <https://www.info.gov.hk/gia/general/202001/20/P2020012000874.htm>) and sulfate level in  $\text{PM}_{2.5}$  was also  
477 lowered by about 30% from 2000 to 2016 (HKEPD, 2017), the roadside  $\text{NO}_2$  level was still high. According to the 20-year air  
478 pollutants monitoring data released by HKSAR, the annual average concentration of roadside  $\text{NO}_2$  was much higher than the  
479 other gaseous pollutants, and it peaked during 2011-2013, which were 122 and 118  $\mu\text{g m}^{-3}$  in 2011 and 2012, respectively.  
480 Although the annual ambient level of roadside  $\text{NO}_2$  decreased to 80  $\mu\text{g m}^{-3}$  in 2019, it is still two times higher than the annual  
481 objective level set by the HKSAR government, indicating a continuous significant impact of  $\text{NO}_x$  on SOA formation in Hong  
482 Kong, especially in areas with heavy traffic load. Given that 90% of the roadside  $\text{NO}_2$  was from commercial vehicles, such as  
483 buses, trucks, minibuses, and so on, our results suggest that more stringent control of  $\text{NO}_x$  emission from commercial vehicles  
484 is needed. This will benefit the community by reducing not only the background  $\text{NO}_x$  levels but also the SOA pollution in  
485 Hong Kong.

#### 486 Appendices

##### 487 Appendix A: Kinetic model of loss of isoprene intermediates

488 In this study, we use Kintecus (Ianni, 2015), a kinetics simulation software, to investigate the degradation pathways of two  
489 isoprene SOA intermediates, i.e., IEPOX and MAE, in the atmosphere. Simulation time was set to be 100 h to ensure the  
490 completion of reactions. As described by Eddingsass et al. (2010) and Worton et al. (2013), IEPOX and MAE are removed  
491 from the atmosphere mainly through three pathways, namely the gas-phase photo-oxidation, dry deposition, and aerosol phase  
492 acid-catalyzed ring-opening reaction. Reaction constants that are involved in these three degradation processes were listed  
493 below.

IEPOX:

$$k_{\text{OX}} = 5.78 \times 10^{-11} \cdot e^{-400/T} \cdot [\text{OH}] \text{ s}^{-1}$$

$$k_{\text{dd}} = dv/\text{blh} \text{ s}^{-1}$$

$$k_{\text{H}^+} = 5 \times 10^{-2} \cdot [\text{H}_3\text{O}^+] \text{ s}^{-1}$$

$$k_{\text{H}}^{\text{cp}} = 1.3 \times 10^8 \text{ M atm}^{-1}$$

MAE:

$$k'_{\text{OX}} = 1.0 \times 10^{-12} \cdot [\text{OH}] \text{ s}^{-1}$$

$$k'_{\text{dd}} = dv/\text{blh} \text{ s}^{-1}$$

$$k'_{\text{H}^+} = 5.91 \times 10^{-5} \cdot [\text{H}_3\text{O}^+] \text{ s}^{-1}$$

$$k'_{\text{H}}^{\text{cp}} = 7.5 \times 10^6 \text{ M atm}^{-1}$$

494 The eight terms, i.e.,  $k_{\text{OX}}$  and  $k'_{\text{OX}}$ ,  $k_{\text{dd}}$  and  $k'_{\text{dd}}$ ,  $k_{\text{H}^+}$  and  $k'_{\text{H}^+}$ , and  $K_{\text{H}}^{\text{cp}}$  and  $K'_{\text{H}}^{\text{cp}}$ , are the gas-phase oxidation rate  
495 constants, dry deposition rate constants, acid-catalyzed ring-opening rate constants, and Henry's law constants of IEPOX and  
496 MAE, respectively. Given the annual average OH radical level in the PRD region was  $5 \times 10^6 \text{ molecules cm}^{-3}$  (Hofzumahaus et  
497 al., 2009),  $k_{\text{OX}}$  and  $k'_{\text{OX}}$  were calculated to be  $7.55 \times 10^{-5} \text{ s}^{-1}$  and  $5.12 \times 10^{-6} \text{ s}^{-1}$  at 298 K.  $k_{\text{dd}}$  is estimated by the deposition  
498 velocity ( $dv$ ) and the boundary layer height ( $blh$ ). Like Eddingsaas et al. (2010) and Worton et al. (2013), we assumed the same  
499 deposition velocities for IEPOX and MAE as that for hydrogen peroxide ( $1\text{-}5 \text{ cm s}^{-1}$ ). With the predicted boundary height in  
500 Hong Kong of 1100 m (Xie et al., 2012),  $k_{\text{dd}}$  and  $k'_{\text{dd}}$  were calculated to be  $5.05 \times 10^{-5} \text{ s}^{-1}$ . Given the high volatility of MAE  
501 vapor pressure ( $9.2 \times 10^{-5} \text{ atm}$ ) (Worton et al., 2013), it has a low tendency to partition onto the particle phase, and its uptake  
502 onto aqueous particles is mainly governed by Henry's law constant ( $k_{\text{H}}^{\text{cp}}$ ). Worton et al. (2013) estimated the  $k_{\text{H}}^{\text{cp}}$  value of  
503 MAE to be  $7.5 \times 10^6 \text{ M atm}^{-1}$ , which is 20 times lower than that of IEPOX ( $1.3 \times 10^8 \text{ M atm}^{-1}$ , Minerath et al., 2008). Moreover,  
504 Riedel et al. (2015) suggested that the heterogeneous reactive uptake coefficient of MAE ( $\gamma = 4.9 \times 10^{-4}$ ) through the ring-  
505 opening reaction was a factor of 30 lower than that of IEPOX. The ring-opening rate constant ( $k_{\text{H}^+}$ ) for IEPOX and MAE were  
506 estimated by Eddingsaas et al. (2010) and Birdsall et al. (2014), which are  $5 \times 10^{-2} \text{ M}^{-1} \text{ s}^{-1}$  and  $5.91 \times 10^{-5} \text{ M}^{-1} \text{ s}^{-1}$ , respectively.  
507 We then inputted all these parameters into the Kintecus model and estimated the fractions of IEPOX and MAE degraded  
508 through the above-mentioned three pathways.

## 509 Appendix B: Calculation of particle acidity and total liquid water content

510 A thermodynamic model (*E-AIM model II*) was applied to estimate the hydrogen ion concentration in air ( $\text{H}^+_{\text{air}}$ ) and liquid  
511 water content associated with inorganic species ( $\text{LWC}_{\text{inorg}}$ ). The liquid water content associated with organic species ( $\text{LWC}_{\text{org}}$ )  
512 was calculated using the following equation

$$513 \text{LWC}_{\text{org}} = \frac{m_{\text{org}} \rho_w}{\rho_{\text{org}}} \frac{k_{\text{org}}}{(1/\text{RH} - 1)}$$

514 where  $k_{\text{org}}$  is an organic hygroscopicity parameter and has a value of 0.1,  $m_{\text{org}}$  is organic mass concentration, and a factor  
515 of 2.1 was applied to convert OC to OM at the urban location.  $\rho_w$  is the water density, and a typical value of  $1.4 \text{ g cm}^{-3}$  was  
516 applied for organic aerosols ( $\rho_{\text{org}}$ ). Since LWC is associated with both inorganic and organic species, the total particle water  
517 ( $\text{LWC}_p$ ) was calculated as the sum of  $\text{LWC}_{\text{inorg}}$  and  $\text{LWC}_{\text{org}}$  based on the assumption that particles were internally well mixed.

518 Particle acidity was calculated using the following equation:

519

$$H_p^+ = \frac{1000H_{air}^+}{LWC_{org} + LWC_{inorg}}$$

520 where  $H_p^+$  ( $\text{mol L}^{-1}$ ) is the concentration of hydrogen ion in aerosol water, interpreted as particle acidity.  $H_{air}^+$  and  $LWC_{inorg}$   
521 were calculated by E-AIM model II using input values of inorganic ions, RH, and temperature.

522 **Data availability.** Raw data used in this study are archived at Hong Kong Baptist University, and are available upon request  
523 by contacting the corresponding author.

524 **Author contributions.** YBC and DH designed the study. YBC did all the experiments and most of the data analysis. YQM  
525 helped with [model-regression](#) analysis and data interpretation. YBC drafted the manuscript. DH helped with data analysis and  
526 interpretation and revised the manuscript.

527 **Competing interest.** The authors declare that they have no conflict of interest.

528

#### 529 **Acknowledgment**

530 This work was supported by the National Natural Science Foundation of China (21976151 and 21477102) and the General  
531 Research Fund of Hong Kong Research Grant Council (12328216, 12304215, 12300914). The authors thank the  
532 Environmental Central Facility (ENVF) in Hong Kong University of Science and Technology (HKUST) for real-time  
533 environmental and air quality data (<http://envf.ust.hk/dataview/gts/current/>).

534 **References**

535 An, Z., Huang, R.J., Zhang, R., Tie, X., Li, G., Cao, J., Zhou, W., Shi, Z., Han, Y., Gu, Z., Ji, Y.: Severe haze in northern China:  
536 A synergy of anthropogenic emissions and atmospheric processes, *Proc. Natl. Acad. Sci. U. S. A.*, 116, 8657–8666,  
537 <https://doi.org/10.1073/pnas.1900125116>, 2019.

538 Barbara J. Finlayson-Pitts, James N. Pitts, J.: Chemistry of the upper and lower atmosphere, Academic Press,  
539 <https://doi.org/https://doi.org/10.1016/B978-0-12-257060-5.X5000-X>, 2000.

540 Birdsall, A.W., Miner, C.R., Mael, L.E., Elrod, M.J.: Mechanistic study of secondary organic aerosol components formed from  
541 nucleophilic addition reactions of methacrylic acid epoxide, *Atmos. Chem. Phys.*, 14, 12951–12964,  
542 <https://doi.org/10.5194/acp-14-12951-2014>, 2014.

543 Brown, S.S., Dubé, W.P., Bahreini, R., Middlebrook, A.M., Brock, C.A., Warneke, C., De Gouw, J.A., Washenfelder, R.A.,  
544 Atlas, E., Peischl, J., Ryerson, T.B., Holloway, J.S., Schwarz, J.P., Spackman, R., Trainer, M., Parrish, D.D., Fehsenfeld,  
545 F.C., Ravishankara, A.R.: Biogenic VOC oxidation and organic aerosol formation in an urban nocturnal boundary layer:  
546 Aircraft vertical profiles in Houston, TX, *Atmos. Chem. Phys.*, 13, 11317–11337. [https://doi.org/10.5194/acp-13-11317-](https://doi.org/10.5194/acp-13-11317-2013)  
547 2013, 2013.

548 Brown, S.S., Dubé, W.P., Tham, Y.J., Zha, Q.Z., Xue, L.K., Poon, S., Wang, Z., Blake, D.R., Tsui, W., Parrish, D.D., Wang, T.:  
549 Nighttime chemistry at a high altitude site above Hong Kong, *J. Geophys. Res. Atmos.*, 121, 2457–2475, doi:10.1002/  
550 2015JD024566, 2016.

551 Bruns, E.A., El Haddad, I., Slowik, J.G., Kilic, D., Klein, F., Baltensperger, U., Prévôt, A.S.H.: Identification of significant  
552 precursor gases of secondary organic aerosols from residential wood combustion, *Sci. Rep.*, 6, 27881.  
553 <https://doi.org/10.1038/srep27881>, 2016.

554 Chan, M.N., Surratt, J.D., Claeys, M., Edgerton, E.S., Tanner, R.L., Shaw, S.L., Zheng, M., Knipping, E.M., Eddingsaas, N.C.,  
555 Wennberg, P.O., Seinfeld, J.H.: Characterization and quantification of isoprene-derived epoxydiols in ambient aerosol  
556 in the southeastern united states, *Environ. Sci. Technol.*, 44, 4590–459, <https://doi.org/10.1021/es100596b>, 2010.

557 Cheng, Y., Ma, Y., Dong, B., Qiu, X., Hu, D.; Pollutants from primary sources dominate the oxidative potential of water-  
558 soluble PM<sub>2.5</sub> in Hong Kong in terms of dithiothreitol (DTT) consumption and hydroxyl radical production. J. Hazard  
559 Mater., 405, 124218, doi:10.1016/j.jhazmat.2020.124218, 2021.

560 Ding, X., Wang, X.M., Gao, B., Fu, X.X., He, Q.F., Zhao, X.Y., Yu, J.Z., Zheng, M.: Tracer-based estimation of secondary  
561 organic carbon in the Pearl River Delta, South China, *J. Geophys. Res. Atmos.*, 117, D05313,  
562 <https://doi.org/10.1029/2011JD016596>, 2012.

563 Ding, X., He, Q., Shen, R., Yu, Q., Wang, X., Guenther, D., Dlugokencky, E., Lang, P., Newberger, T., Wolter, S., White, A.,  
564 Noone, D., Wolfe, D., Schnell, R., Ding, X., He, Q., Shen, R., Yu, Q., Wang, X.: Spatial distributions of secondary  
565 organic aerosols from isoprene, monoterpenes, β-caryophyllene, and aromatics over China during summer, *J. Geophys.*  
566 *Res. Atmos.*, 119, 11877–11891, <https://doi.org/10.1002/2014JD02174>, 2014.

567 Eddingsaas, N.C., Vandervelde, D.G., Wennberg, P.O.: Kinetics and products of the acid-catalyzed ring-opening of  
568 atmospherically relevant butyl epoxy alcohols, *J. Phys. Chem. A*, 114, 8106–8113, <https://doi.org/10.1021/jp103907c>,  
569 2010.

570 Ehn, M., Thornton, J.A., Kleist, E., Sipilä, M., Junninen, H., Pullinen, I., Springer, M., Rubach, F., Tillmann, R., Lee, B.,  
571 Lopez-Hilfiker, F., Andres, S., Acir, I.H., Rissanen, M., Jokinen, T., Schobesberger, S., Kangasluoma, J., Kontkanen, J.,  
572 Nieminen, T., Kurtén, T., Nielsen, L.B., Jørgensen, S., Kjaergaard, H.G., Canagaratna, M., Maso, M.D., Berndt, T., Petäjä,  
573 T., Wahner, A., Kerminen, V.M., Kulmala, M., Worsnop, D.R., Wildt, J., Mentel, T.F.: A large source of low-volatility  
574 secondary organic aerosol, *Nature*, 506, 476–479, <https://doi.org/10.1038/nature13032>, 2014.

575 Environmental Protection Department of Hong Kong, Hong Kong emission inventory report.  
576 [https://www.epd.gov.hk/epd/sc\\_chi/environmentinhk/air/data/emission\\_inve.html](https://www.epd.gov.hk/epd/sc_chi/environmentinhk/air/data/emission_inve.html), 2017.

Formatted: Font: (Default) Times New Roman, 10 pt, Not Bold

Formatted: No underline

Formatted: Font: (Default) Times New Roman, 10 pt, Not Bold

Formatted: Font: (Default) Times New Roman, 10 pt, Not Bold, Not Italic

Formatted: Font: (Default) Times New Roman, 10 pt, Not Bold, Not Italic

Formatted: Font: (Default) Times New Roman, 10 pt, Not Bold, Not Italic

Formatted: Font: (Default) Times New Roman, 10 pt, Not Bold

Formatted: Font: (Default) Times New Roman, 10 pt, Not Bold

Formatted: Font: 9 pt

577 Finewax, Z., De Gouw, J.A., Ziemann, P.J.: Identification and quantification of 4-nitrocatechol formed from OH and NO<sub>3</sub>  
578 radical-initiated reactions of catechol in air in the presence of NO<sub>x</sub>: Implications for secondary organic aerosol formation  
579 from biomass burning, *Environ. Sci. Technol.*, 52, 1981–1989, <https://doi.org/10.1021/acs.est.7b05864>, 2018.

580 Fry, J.L., Rollins, W., Wooldridge, P.J., Brown, S.S., Fuchs, H., Dub, W.: Organic nitrate and secondary organic aerosol  
581 yield from NO<sub>3</sub> oxidation of β-pinene evaluated using a gas-phase kinetics/aerosol partitioning model, *Atmos. Chem.  
582 Phys.*, 9, 1431–1449, <https://doi.org/10.5194/acp-9-1431-2009>, 2009.

583 Fu, P., Kawamura, K., Chen, J., Miyazaki, Y.: Secondary production of organic aerosols from biogenic VOCs over Mt. Fuji,  
584 Japan, *Environ. Sci. Technol.*, 48, 8491–8497, <https://doi.org/10.1021/es500794d>, 2014.

585 Gelencsér, A., May, B., Simpson, D., Sánchez-Ochoa, A., Kasper-Giebl, A., Puxbaum, H., Caseiro, A., Pio, C.A., Legrand, M.:  
586 Source apportionment of PM<sub>2.5</sub> organic aerosol over Europe: Primary/secondary, natural/anthropogenic, and  
587 fossil/biogenic origin, *J. Geophys. Res. Atmos.* 112, 1–12, <https://doi.org/10.1029/2006JD008094>, 2007.

588 He, Q.F., Ding, X., Fu, X.X., Zhang, Y.Q., Wang, J.Q., Liu, Y.X., Tang, M.J., Wang, X.M., Rudich, Y., Secondary organic  
589 aerosol formation from isoprene epoxides in the Pearl River Delta, South China: IEPOX- and HMML-derived tracers,  
590 *J. Geophys. Res. Atmos.*, 123, 6999–7012, <https://doi.org/10.1029/2017JD028242>, 2018.

591 He, X., Huang, X.H.H., Chow, K.S., Wang, Q., Zhang, T., Wu, D., Yu, J.Z.: Abundance and sources of phthalic acids, benzene-  
592 tricarboxylic acids, and phenolic acids in PM<sub>2.5</sub> at urban and suburban sites in Southern China, *ACS Earth Sp. Chem.*, 2,  
593 147–158, <https://doi.org/10.1021/acsearthspacechem.7b00131>, 2018.

594 Hildemann, L.M., Rogge, W.F., Cass, G.R., Mazurek, M.A., Simoneit, B.R.T.: Contribution of primary aerosol emissions from  
595 vegetation-derived sources to fine particle concentrations in Los Angeles, *J. Geophys. Res.*, 101, 19541,  
596 <https://doi.org/10.1029/95JD02136>, 1996.

597 Hofzumahaus, A., Rohrer, F., Lu, K., Bohn, B., Brauers, T., Chang, C.-C., Fuchs, H., Holland, F., Kita, K., Kondo, Y., Li, X.,  
598 Lou, S., Shao, M., Zeng, L., Wahner, A., Zhang, Y.: Amplified trace gas removal in the troposphere, *Science*, 324, 1702–  
599 1704, <https://doi.org/10.1126/science.1164566>, 2009.

600 Hu, D., Yu, J. Z.: Secondary organic aerosol tracers and malic acid in Hong Kong: Seasonal trends and origins, *Environ. Chem.*,  
601 10, 381–394, <https://doi.org/10.1071/EN13104>, 2013.

602 Hu, D., Bian, Q., Li, T.W.Y., Lau, A.K.H., Yu, J.Z.: Contributions of isoprene, monoterpenes, β-caryophyllene, and toluene to  
603 secondary organic aerosols in Hong Kong during the summer of 2006, *J. Geophys. Res. Atmos.*, 113,  
604 <https://doi.org/10.1029/2008JD010437>, 2008.

605 Hu, D., Bian, Q., Lau, A.K.H., Yu, J.Z.: Source apportionment of primary and secondary organic carbon in summer PM<sub>2.5</sub> in  
606 Hong Kong using positive matrix factorization of secondary and primary organic tracer data, *J. Geophys. Res. Atmos.*,  
607 115, 1–14, <https://doi.org/10.1029/2009JD012498>, 2010.

608 Huang, R.J., Zhang, Y., Bozzetti, C., Ho, K.F., Cao, J.J., Han, Y., Daellenbach, K.R., Slowik, J.G., Platt, S.M., Canonaco, F.,  
609 Zotter, P., Wolf, R., Pieber, S.M., Bruns, E.A., Crippa, M., Ciarelli, G., Piazzalunga, A., Schwikowski, M., Abbaszade,  
610 G., Schnelle-Kreis, J., Zimmermann, R., An, Z., Szidat, S., Baltensperger, U., El Haddad, I., Prevot, A.S.: High secondary  
611 aerosol contribution to particulate pollution during haze events in China, *Nature*, 514, 218–222,  
612 <https://doi.org/10.1038/nature13774>, 2014.

613 [Ianni, J.C.: KINTECUS, Windows version 5.50, 2015.](#)

614 Jang, M., Czoschke, N.M., Lee, S., Kamens, R.M.: Heterogeneous atmospheric aerosol production by acid-catalyzed particle-  
615 phase reactions, *Science*, 298, 814–817, <https://doi.org/10.1126/science.1075798>, 2002.

616 Jaoui, M., Kleindienst, T.E., Lewandowski, M., Offenberg, J.H., Edney, E.O.: Identification and quantification of aerosol polar  
617 oxygenated compounds bearing carboxylic or hydroxyl groups. 2. Organic tracer compounds from monoterpenes,  
618 *Environ. Sci. Technol.*, 39, 5661–5673, <https://doi.org/10.1021/es048111b>, 2005.

619 Jokinen, T., Berndt, T., Makkonen, R., Kerminen, V.M., Junninen, H., Paasonen, P., Stratmann, F., Herrmann, H., Guenther,

Formatted: Indent: Left: 0", First line: 0", Adjust space between Latin and Asian text, Adjust space between Asian text and numbers

620 A.B., Worsnop, D.R., Kulmala, M., Ehn, M., Sipilä, M.: Production of extremely low volatile organic compounds from  
621 biogenic emissions: Measured yields and atmospheric implications, *Proc. Natl. Acad. Sci. U. S. A.*, 112, 7123–7128,  
622 <https://doi.org/10.1073/pnas.1423977112>, 2015.

623 Kanakidou, M., Seinfeld, J.H., Pandis, S.N., Barnes, I., Dentener, F.J., Facchini, M.C., Van Dingenen, R., Ervens, B., Nenes,  
624 A., Nielsen, C.J., Swietlicki, E., Putaud, J.P., Balkanski, Y., Fuzzi, S., Horth, J., Moortgat, G.K., Winterhalter, R., Myhre,  
625 C.E.L., Tsigaridis, K., Vignati, E., Stephanou, E.G., Wilson, J.: Organic aerosol and global climate modelling: a review,  
626 *Atmos. Chem. Phys.*, 5, 1053–1123, <https://doi.org/10.5194/acp-5-1053-2005>, 2005.

627 Kautzman, K.E., Surratt, J.D., Chan, M.N., Chan, A.W.H., Hersey, S.P., Chhabra, P.S., Dalleska, N.F., Wennberg, P.O., Flagan,  
628 R.C., Seinfeld, J.H.: Chemical composition of gas- and aerosol-phase products from the photooxidation of naphthalene,  
629 *J. Phys. Chem. A*, 114, 913–934, <https://doi.org/10.1021/jp908530s>, 2010.

630 Kenseth, C.M., Huang, Y., Zhao, R., Dalleska, N.F., Caleb Hethcox, J., Stoltz, B.M., Seinfeld, J.H.: Synergistic O<sub>3</sub>+OH  
631 oxidation pathway to extremely low-volatility dimers revealed in β-pinene secondary organic aerosol, *Proc. Natl. Acad.*  
632 *Sci. U. S. A.*, 115, 8301–8306, <https://doi.org/10.1073/pnas.1804671115>, 2018.

633 Kitanovski, Z., Grgić, I., Vermeylen, R., Claeys, M., Maenhaut, W.: Liquid chromatography tandem mass spectrometry method  
634 for characterization of monoaromatic nitro-compounds in atmospheric particulate matter, *J. Chromatogr. A*, 1268, 35–  
635 43, <https://doi.org/10.1016/j.chroma.2012.10.021>, 2012.

636 Kleindienst, T.E., Jaoui, M., Lewandowski, M., Offenberg, J.H., Lewis, C.W., Bhawe, P. V., Edney, E.O.: Estimates of the  
637 contributions of biogenic and anthropogenic hydrocarbons to secondary organic aerosol at a southeastern US location,  
638 *Atmos. Environ.*, 41, 8288–8300, <https://doi.org/10.1016/j.atmosenv.2007.06.045>, 2007.

639 Kleindienst, T.E., Lewandowski, M., Offenberg, J.H., Jaoui, M., Edney, E.O.: The formation of secondary organic aerosol  
640 from the isoprene + OH reaction in the absence of NO<sub>x</sub>, *Atmos. Chem. Phys.*, 9, 6541–6558, [https://doi.org/10.5194/acp-](https://doi.org/10.5194/acp-9-6541-2009)  
641 [9-6541-2009](https://doi.org/10.5194/acp-9-6541-2009), 2009.

642 Kleindienst, T.E., Jaoui, M., Lewandowski, M., Offenberg, J.H., Docherty, K.S.: The formation of SOA and chemical tracer  
643 compounds from the photo-oxidation of naphthalene and its methyl analogs in the presence and absence of nitrogen  
644 oxides, *Atmos. Chem. Phys.*, 12, 8711–8726, <https://doi.org/10.5194/acp-12-8711-2012>, 2012.

645 Lee, A., Goldstein, A.H., Keywood, M.D., Gao, S., Varutbangkul, V., Bahreini, R., Ng, N.L., Flagan, R.C., Seinfeld, J.H.: Gas-  
646 phase products and secondary aerosol yields from the ozonolysis of ten different terpenes, *J. Geophys. Res. Atmos.*, 111,  
647 1–18, <https://doi.org/10.1029/2005JD006437>, 2006a.

648 Lee, A., Goldstein, A.H., Kroll, J.H., Ng, N.L., Varutbangkul, V., Flagan, R.C., Seinfeld, J.H.: Gas-phase products and  
649 secondary aerosol yields from the photo-oxidation of 16 different terpenes, *J. Geophys. Res. Atmos.*, 111, D17305,  
650 <https://doi.org/10.1029/2006JD007050>, 2006b.

651 Lewandowski, M., Jaoui, M., Offenberg, J.H., Kleindienst, T.E., Edney, E.O., Sheesley, R. J., Schauer, J.J.: Primary and  
652 secondary contributions to ambient PM in the midwestern united states, *Environ. Sci. Technol.*, 42, 3303–3309,  
653 <https://doi.org/10.1021/es0720412>, 2008.

654 Lin, Y.-H., Zhang, Z., Docherty, K.S., Zhang, H., Budisulistiorini, S.H., Rubitschun, C.L., Shaw, S.L., Knipping, E.M.,  
655 Edgerton, E.S., Kleindienst, T.E., Gold, A., Surratt, J.D.: Isoprene epoxydiols as precursors to secondary organic aerosol  
656 formation: Acid-catalyzed reactive uptake studies with authentic compounds, *Environ. Sci. Technol.*, 46, 250–258,  
657 <https://doi.org/10.1021/es202554c>, 2012.

658 Lin, Y.-H., Zhang, H., Pye, H.O.T., Zhang, Z., Marth, W.J., Park, S., Arashiro, M., Cui, T., Budisulistiorini, S.H., Sexton, K.G.,  
659 Vizuete, W., Xie, Y., Luecken, D.J., Piletic, I.R., Edney, E.O., Bartolotti, L.J., Gold, A., Surratt, J.D.: Epoxide as a  
660 precursor to secondary organic aerosol formation from isoprene photo-oxidation in the presence of nitrogen oxides, *Proc.*  
661 *Natl. Acad. Sci. U. S. A.*, 110, 6718–6723, <https://doi.org/10.1073/pnas.1221150110>, 2013.

662 Lu, X., Fung, J.: Source apportionment of sulfate and nitrate over the Pearl River Delta Region in China, *Atmosphere*, 7, 98,

663 <https://doi.org/10.3390/atmos7080098>, 2016.

664 Ma, Y., Cheng, Y., Qiu, X., Lin, Y., Cao, J., Hu, D.: A quantitative assessment of source contributions to fine particulate matter  
665 (PM<sub>2.5</sub>)-bound polycyclic aromatic hydrocarbons (PAHs) and their nitrated and hydroxylated derivatives in Hong Kong,  
666 *Environ. Pollut.*, 219, 742-749, <https://doi.org/10.1016/j.envpol.2016.07.034>, 2016.

667 Ma, Y., Cheng, Y., Qiu, X., Cao, G., Fang, Y., Wang, J., Zhu, T., Yu, J., Hu, D.: Sources and oxidative potential of water-soluble  
668 humic-like substances (HULIS<sub>WS</sub>) in fine particulate matter (PM<sub>2.5</sub>) in Beijing, *Atmos. Chem. Phys.*, 18, 5607-5617,  
669 <https://doi.org/10.5194/acp-18-5607-2018>, 2018.

670 Ma, Y., Cheng, Y., Qiu, X., Cao, G., Kuang, B., Yu, J.Z., Hu, D.: Optical properties-, source apportionment and redox activity  
671 of humic-like substances (HULIS) in airborne fine particulates in Hong Kong, *Environ. Pollut.*, 255, 113087,  
672 <https://doi.org/10.1016/j.envpol.2019.113087>, 2019.

673 Mancilla, Y., Herckes, P., Fraser, M.P., Mendoza, A.: Secondary organic aerosol contributions to PM<sub>2.5</sub> in Monterrey, Mexico:  
674 Temporal and seasonal variation, *Atmos. Res.*, 153, 348-359, <https://doi.org/10.1016/j.atmosres.2014.09.009>, 2015.

675 Minerath, E. C., Casale, M. T., Elrod, M. J.: Kinetics feasibility study of alcohol sulfate esterification reactions in tropospheric  
676 aerosols, *Environ. Sci. Technol.*, 42, 4410-4415, <https://doi.org/10.1021/es8004333>, 2008.

677 Ng, N.L., Kwan, A.J., Surratt, J.D., Chan, A.W.H., Chhabra, P.S., Sorooshian, A., Pye, H.O.T., Crounse, J.D., Wennberg, P.O.,  
678 Flagan, R.C., Seinfeld, J.H.: Secondary organic aerosol (SOA) formation from reaction of isoprene with nitrate radicals  
679 (NO<sub>3</sub>), *Atmos. Chem. Phys.*, 8, 4117-4140, <https://doi.org/10.5194/acp-8-4117-2008>, 2008.

680 Nguyen, T.B., Bates, K.H., Crounse, J.D., Schwantes, R.H., Zhang, X., Kjaergaard, H.G., Surratt, J.D., Lin, P., Laskin, A.,  
681 Seinfeld, J.H., Wennberg, P.O.: Mechanism of the hydroxyl radical oxidation of methacryloyl peroxyxynitrate (MPAN)  
682 and its pathway toward secondary organic aerosol formation in the atmosphere, *Phys. Chem. Chem. Phys.*, 17, 17914-  
683 17926, <https://doi.org/10.1039/c5cp02001h>, 2015.

684 Offenberg, J. H., Lewis, C. W., Lewandowski, M., Jaoui, M., Kleindienst, T. E., Edney, E. O.: Contributions of toluene and  $\alpha$ -  
685 pinene to SOA formed in an irradiated toluene/ $\alpha$ -pinene/NO<sub>x</sub>/air mixture: comparison of results using <sup>14</sup>C content and  
686 SOA organic tracer methods, *Environ. Sci. Technol.*, 41, 3972-3976, <https://doi.org/10.1021/es070089>, 2007.

687 Rattanavaraha, W., Chu, K., Budisulistiorini, S.H., Riva, M., Lin, Y.H., Edgerton, E.S., Baumann, K., Shaw, S.L., Guo, H.,  
688 King, L., Weber, R.J., Neff, M.E., Stone, E.A., Offenberg, J.H., Zhang, Z., Gold, A., Surratt, J.D.: Assessing the impact  
689 of anthropogenic pollution on isoprene-derived secondary organic aerosol formation in PM<sub>2.5</sub> collected from the  
690 Birmingham, Alabama, ground site during the 2013 Southern Oxidant and Aerosol Study, *Atmos. Chem. Phys.*, 16,  
691 4897-4914, <https://doi.org/10.5194/acp-16-4897-2016>, 2016.

692 Riedel, T.P., Lin, Y.H., Budisulistiorini, S.H., Gaston, C.J., Thornton, J.A., Zhang, Z., Vizuete, W., Gold, A., Surratt, J.D.:  
693 Heterogeneous reactions of isoprene-derived epoxides: Reaction probabilities and molar secondary organic aerosol yield  
694 estimates, *Environ. Sci. Technol. Lett.*, 2, 38-42, <https://doi.org/10.1021/ez500406f>, 2015.

695 Riva, M., Tomaz, S., Cui, T., Lin, Y.H., Perraudin, E., Gold, A., Stone, E.A., Villenave, E., Surratt, J.D.: Evidence for an  
696 unrecognized secondary anthropogenic source of organosulfates and sulfonates: Gas-phase oxidation of polycyclic  
697 aromatic hydrocarbons in the presence of sulfate aerosol, *Environ. Sci. Technol.*, 49, 6654-6664,  
698 <https://doi.org/10.1021/acs.est.5b00836>, 2015.

699 Roberts, J.M., Bertman, S.B.: The thermal decomposition of peroxyacetic nitric anhydride (PAN) and peroxyacetic nitric  
700 anhydride (MPAN), *Int. J. Chem. Kinet.*, 24, 297-307, <https://doi.org/10.1002/kin.550240307>, 1992.

701 Rollins, A.W., Pusede, S., Wooldridge, P., Min, K.-E., Gentner, D. R., Goldstein, A.H., Liu, S., Day, D. A., Russell, L. M.,  
702 Rubitschun, C. L., Surratt, J. D., Cohen, R.C.: Gas particle partitioning of total alkyl nitrates observed with TD-LIF in  
703 Bakersfield, *J. Geophys. Res. Atmos.*, 118, 6651-6662, <https://doi.org/10.1002/jgrd.50522>, 2013.

704 Sang, X.F., Chan, C.Y., Engling, G., Chan, L.Y., Wang, X.M., Zhang, Y.N., Shi, S., Zhang, Z.S., Zhang, T., Hu, M.:  
705 Levoglucosan enhancement in ambient aerosol during springtime transport events of biomass burning smoke to

706 Southeast China, *Tellus B*, 63, 129–139, <https://doi.org/10.1111/j.1600-0889.2010.00515.x>, 2011.

707 Schauer, J.J., Kleeman, M.J., Cass, G.R., Simoneit, B.R.T.: Measurement of emissions from air pollution sources. 3. C<sub>1</sub>-C<sub>29</sub>  
708 organic compounds from fireplace combustion of wood, *Environ. Sci. Technol.*, 35, 1716–1728,  
709 <https://doi.org/10.1021/es001331e>, 2001.

710 Schauer, J.J., Rogge, W.F., Hildemann, L.M., Mazurek, M.A., Cass, G.R., Simoneit, B.R.T.: Source apportionment of airborne  
711 particulate matter using organic compounds as tracers, *Atmos. Environ.*, 41, 241–259,  
712 <https://doi.org/10.1016/j.atmosenv.2007.10.069>, 2007.

713 Simoneit, B.R.T.: A review of biomarker compounds as source indicators and tracers for air pollution, *Environ. Sci. Pollut.*  
714 *Res.*, 6, 159–169, <https://doi.org/10.1007/BF02987621>, 1999.

715 Simoneit, B.R.T., Medeiros, P.M., Didyk, B.M.: Combustion products of plastics as indicators for refuse burning in the  
716 atmosphere, *Environ. Sci. Technol.*, 39, 6961–6970, <https://doi.org/10.1021/es050767x>, 2005.

717 Surratt, J.D., Chan, A.W.H., Eddingsaas, N.C., Chan, M., Loza, C.L., Kwan, A.J., Hersey, S.P., Flagan, R.C., Wennberg, P.O.,  
718 Seinfeld, J.H.: Reactive intermediates revealed in secondary organic aerosol formation from isoprene, *Proc. Natl. Acad.*  
719 *Sci. U. S. A.*, 107, 6640–6645, <https://doi.org/10.1073/pnas.0911114107>, 2010.

720 Tsui, J.K.Y., Guenther, A., Yip, W.K., Chen, F.: A biogenic volatile organic compound emission inventory for Hong Kong,  
721 *Atmos. Environ.*, 43, 6442–6448, <https://doi.org/10.1016/j.atmosenv.2008.01.027>, 2009.

722 Van Dingenen, R., Raes, F., Putaud, J.P., Baltensperger, U., Charron, A., Facchini, M.C., Decesari, S., Fuzzi, S., Gehrig, R.,  
723 Hansson, H.C., Harrison, R.M., Hüglin, C., Jones, A.M., Laj, P., Lorbeer, G., Maenhaut, W., Palmgren, F., Querol, X.,  
724 Rodriguez, S., Schneider, J., Ten Brink, H., Tunved, P., Tørseth, K., Wehner, B., Weingartner, E., Wiedensohler, A.,  
725 Wählin, P.: A European aerosol phenomenology-1: Physical characteristics of particulate matter at kerbside, urban, rural  
726 and background sites in Europe, *Atmos. Environ.*, 38, 2561–2577, <https://doi.org/10.1016/j.atmosenv.2004.01.040>, 2004.

727 Viana, M., Amato, F., Alastuey, A., Querol, X., Moreno, T., Dos Santos, S.G., Hecce, M.D., Fernández-Patier, R.: Chemical  
728 tracers of particulate emissions from commercial shipping, *Environ. Sci. Technol.*, 43, 7472–7477,  
729 <https://doi.org/10.1021/es901558t>, 2009.

730 Vione, D., Maurino, V., Minero, C., Pelizzetti, E.: Phenol photomnitration upon UV irradiation of nitrite in aqueous solution II:  
731 Effects of pH and TiO<sub>2</sub>, *Chemosphere*, 45, 903–910, [https://doi.org/10.1016/S0045-6535\(01\)00036-4](https://doi.org/10.1016/S0045-6535(01)00036-4), 2001.

732 Wang, G., Zhang, R., Gomez, M.E., Yang, L., Zamora, M.L., Hu, M., Lin, Y., Peng, J., Guo, S., Meng, J., Li, J., Cheng, C.,  
733 Hu, T., Ren, Y., Wang, Y.Y., Gao, J., Cao, J., An, Z., Zhou, W., Li, G., Wang, J., Tian, P., Marrero-Ortiz, W., Secrest, J.,  
734 Du, Z., Zheng, J., Shang, D., Zeng, L., Shao, M., Wang, W., Huang, Y., Wang, Y.Y., Zhu, Y., Li, Y., Hu, J., Pan, B., Cai,  
735 L., Cheng, Y., Ji, Y., Zhang, F., Rosenfeld, D., Liss, P.S., Duce, R.A., Kolb, C.E., Molina, M.J., Peng, J., Duan, L., Ji, Y.,  
736 Marrero-Ortiz, W., An, Z., Huang, R., Zhang, R., Tie, X., Li, G., Cao, J.: Persistent sulfate formation from London Fog  
737 to Chinese haze, *Proc. Natl. Acad. Sci. U. S. A.*, 113, 13630–13635, <https://doi.org/10.1073/pnas.1616540113>, 2016.

738 Worton, D.R., Surratt, J.D., LaFranchi, B.W., Chan, A.W.H., Zhao, Y., Weber, R.J., Park, J.-H., Gilman, J.B., De Gouw, J.,  
739 Park, C., Schade, G., Beaver, M.R., St. Clair, J., Crounse, J.D., Wennberg, P., Wolfe, G.M., Harrold, S., Thornton, J.,  
740 Farmer, D., Docherty, K.S., Cubison, M., Jimenez, J.L., Frossard, A., Russell, L.M., Kristensen, K., Glasius, M., Mao,  
741 J., Ren, X., Brune, B., Browne, E.C., Pusede, S., Cohen, R.C., Seinfeld, J.H., Goldstein, A.H.: Observational insights  
742 into high- and low-NO<sub>x</sub> aerosol formation from isoprene, *Environ. Sci. Technol.*, 47, 11403–11413,  
743 <https://doi.org/10.1021/es4011064>, 2013.

744 Xie, B., Fung, J. C. H., Chan, A., Lau, A.: Evaluation of nonlocal and local planetary boundary layer schemes in the WRF  
745 model, *J. Geophys. Res. Atmos.*, 117, D12103, <https://doi.org/10.1029/2011JD017080>, 2012.

746 Xu, L., Guo, H., Boyd, C.M., Klein, M., Bougiatioti, A., Cerully, K.M., Hite, J.R., Isaacman-VanWertz, G., Kreisberg, N.M.,  
747 Knote, C., Olson, K., Koss, A., Goldstein, A.H., Hering, S. V., de Gouw, J., Baumann, K., Lee, S.-H., Nenes, A., Weber,  
748 R.J., Ng, N.L.: Effects of anthropogenic emissions on aerosol formation from isoprene and monoterpenes in the

749 southeastern United States, *Proc. Natl. Acad. Sci. U. S. A.*, 112, 37–42, <https://doi.org/10.1073/pnas.1417609112>, 2015.

750 Yu, J.Z., Huang, X.-F., Xu, J., Hu, M.: When aerosol sulfate goes up, so does oxalate: Implication for the formation  
751 mechanisms of oxalate, *Environ. Sci. Technol.*, 39, 128–133, <https://doi.org/10.1021/es049559f>, 2005.

752 Yu, L., Smith, J., Laskin, A., Anastasio, C., Laskin, J., Zhang, Q.: Chemical characterization of SOA formed from aqueous-  
753 phase reactions of phenols with the triplet excited state of carbonyl and hydroxyl radical, *Atmos. Chem. Phys.*, 14,  
754 13801–13816, <https://doi.org/10.5194/acp-14-13801-2014>, 2014.

755 Yuan, Z.B., Yu, J.Z., Lau, A.K.H., Louie, P.K.K., Fung, J.C.H.: Application of positive matrix factorization in estimating  
756 aerosol secondary organic carbon in Hong Kong and its relationship with secondary sulfate, *Atmos. Chem. Phys.*, 6, 25–  
757 34, <https://doi.org/10.5194/acp-6-25-2006>, 2006.

758 Worton, D.R., Surratt, J.D., LaFranchi, B.W., Chan, A.W.H., Zhao, Y., Weber, R.J., Park, J.-H., Gilman, J.B., De Gouw, J.,  
759 Park, C., Schade, G., Beaver, M.R., StClair, J., Crounse, J.D., Wennberg, P., Wolfe, G.M., Harrold, S., Thornton, J.,  
760 Farmer, D., Docherty, K.S., Cubison, M., Jimenez, J.L., Frossard, A. a, Russell, L.M., Kristensen, K., Glasius, M., Mao,  
761 J., Ren, X., Brune, B., Browne, E.C., Pusede, S., Cohen, R.C., Seinfeld, J.H., Goldstein, A.H.: Observational insights  
762 into high- and low-NO<sub>x</sub> aerosol formation from isoprene, *Environ. Sci. Technol.*, 47, 11403–11413,  
763 <https://doi.org/10.1021/es4011064>, 2013.

764 Zhang, H., Yee, L.D., Lee, B.H., Curtis, M.P., Worton, D.R., Isaacman-VanWertz, G., Offenberg, J.H., Lewandowski, M.,  
765 Kleindienst, T.E., Beaver, M.R., Holder, A.L., Lonneman, W.A., Docherty, K.S., Jaoui, M., Pye, H.O.T., Hu, W., Day,  
766 D.A., Campuzano-Jost, P., Jimenez, J.L., Guo, H., Weber, R.J., De Gouw, J., Koss, A.R., Edgerton, E.S., Brune, W.,  
767 Mohr, C., Lopez-Hilfiker, F.D., Lutz, A., Kreisberg, N.M., Spielman, S.R., Hering, S. V., Wilson, K.R., Thornton, J.A.,  
768 Goldstein, A.H.: Monoterpenes are the largest source of summertime organic aerosol in the southeastern United States,  
769 *Proc. Natl. Acad. Sci. U. S. A.*, 115, 2038–2043, <https://doi.org/10.1073/pnas.1717513115>, 2018.

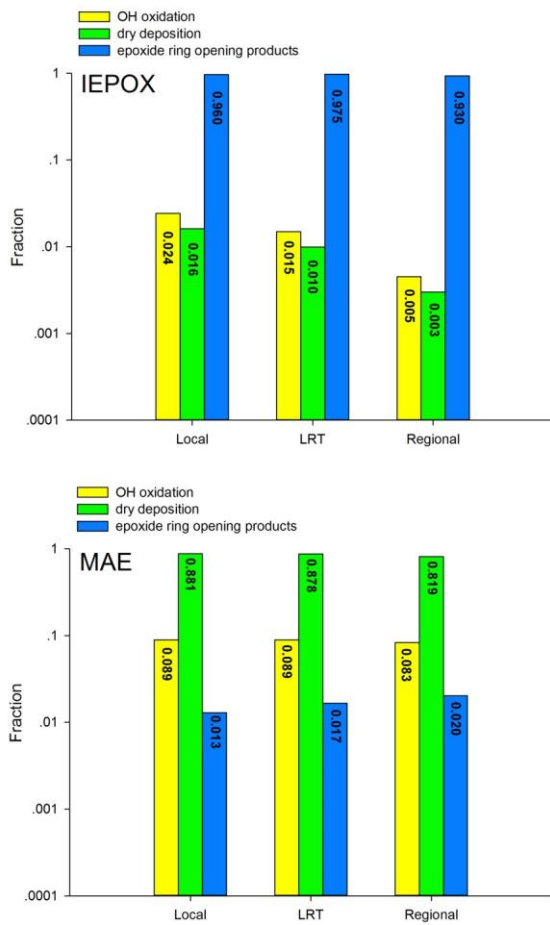
770 Zhang, Q., Jimenez, J.L., Canagaratna, M.R., Allan, J.D., Coe, H., Ulbrich, I., Alfarra, M.R., Takami, A., Middlebrook, A.M.,  
771 Sun, Y.L., Dzepina, K., Dunlea, E., Docherty, K., DeCarlo, P.F., Salcedo, D., Onasch, T., Jayne, J.T., Miyoshi, T.,  
772 Shimono, A., Hatakeyama, S., Takegawa, N., Kondo, Y., Schneider, J., Drewnick, F., Borrmann, S., Weimer, S.,  
773 Demerjian, K., Williams, P., Bower, K., Bahreini, R., Cottrell, L., Griffin, R.J., Rautiainen, J., Sun, J.Y., Zhang, Y.M.,  
774 Worsnop, D.R.: Ubiquity and dominance of oxygenated species in organic aerosols in anthropogenically-influenced  
775 Northern Hemisphere midlatitudes, *Geophys. Res. Lett.*, 34, 1–6, <https://doi.org/10.1029/2007GL029979>, 2007.

776 Zhang, T., Claeys, M., Cachier, H., Dong, S., Wang, W., Maenhaut, W., Liu, X.: Identification and estimation of the biomass  
777 burning contribution to Beijing aerosol using levoglucosan as a molecular marker, *Atmos. Environ.*, 42, 7013–7021,  
778 <https://doi.org/10.1016/j.atmosenv.2008.04.050>, 2008.

779 Zhang, Y. X., Shao, M., Zhang, Y.H., Zeng, L.M., He, L.Y., Zhu, B., Wei, Y.J., Zhu, X.L.: Source profiles of particulate organic  
780 matters emitted from cereal straw burnings, *J. Environ. Sci.*, 19, 167–175, [https://doi.org/10.1016/S1001-0742\(07\)60027-8](https://doi.org/10.1016/S1001-0742(07)60027-8), 2007.

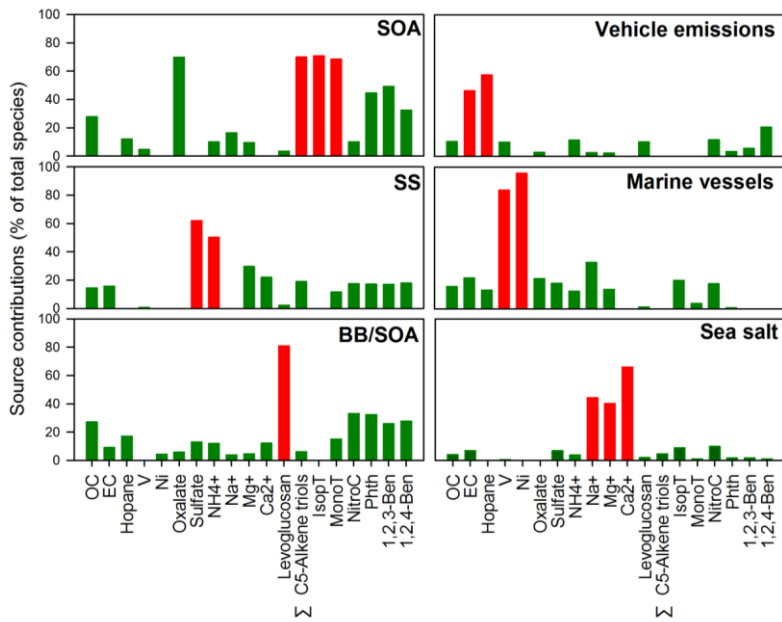
782 Zheng, M., Salmon, L.G., Schauer, J.J., Zeng, L., Kiang, C.S., Zhang, Y., Cass, G.R.: Seasonal trends in PM<sub>2.5</sub> source  
783 contributions in Beijing, China, *Atmos. Environ.*, 39, 3967–3976, <https://doi.org/10.1016/j.atmosenv.2005.03.036>, 2005.

784 Zheng, M., Zhao, X., Cheng, Y., Yan, C., Shi, W., Zhang, X., Weber, R.J., Schauer, J.J., Wang, X., Edgerton, E.S.: Sources of  
785 primary and secondary organic aerosol and their diurnal variations, *J. Hazard. Mater.*, 264, 536–544,  
786 <https://doi.org/10.1016/j.jhazmat.2013.10.047>, 2014.



787

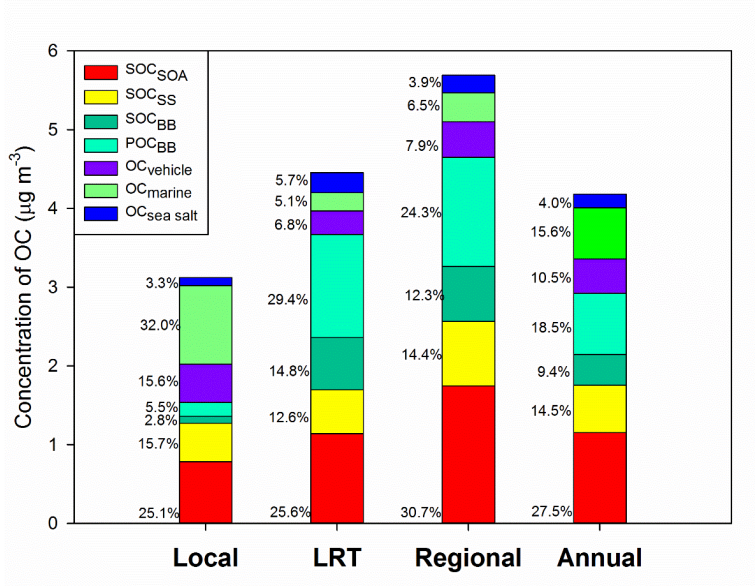
788 Figure 1: Comparison of three degradation processes for IEPOX and MAE under the three synoptic conditions



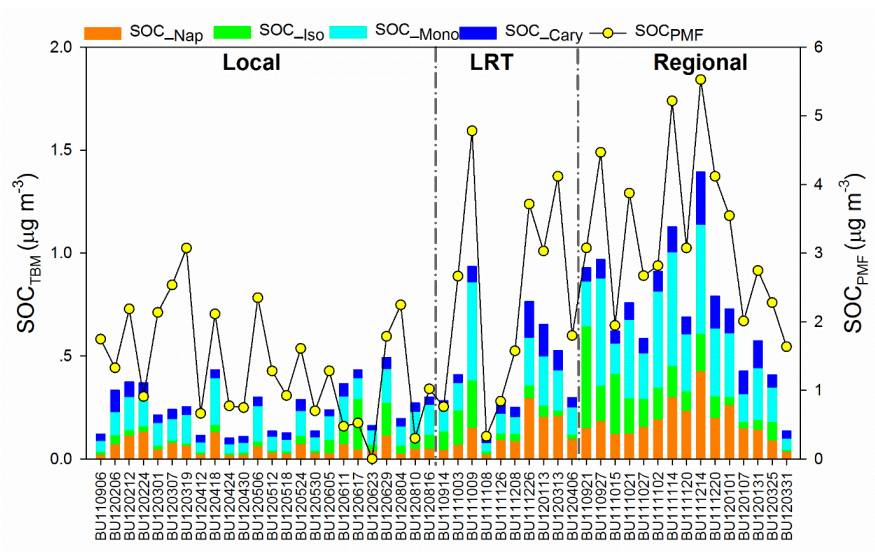
789

790 Figure 2: PMF-resolved source contributions (% of total species) to ambient PM<sub>2.5</sub> samples collected in Hong Kong. Red  
 791 column: chemical markers for source identification.

792



793  
 794 Figure 3: Source-specific contributions to OC under different meteorological conditions. OC<sub>BB</sub> was split into POC<sub>BB</sub> and  
 795 SOC<sub>BB</sub>.



796  
 797 Figure 4: Temporal variations of SOC<sub>PMF</sub> and SOC<sub>TBM</sub>.

Table 1: Concentrations of 15 SOA tracers, 25 polar organic compounds, and nine inorganic ions in PM<sub>2.5</sub> collected in Hong Kong under three meteorological conditions.

|  | Local (N=24) |             | Long regional transport (N=10) |             | Regional (N=15) |             |
|--|--------------|-------------|--------------------------------|-------------|-----------------|-------------|
|  | Average      | Range       | Average                        | Range       | Average         | Range       |
| <i>Tracers for isoprene SOA (ng m<sup>-3</sup>)</i>        |              |             |                                |             |                 |             |
| 2-Methylglyceric acid                                      | 0.56±0.31    | 0.22-1.42   | 1.28±0.86                      | 0.29-2.61   | 2.36±1.75       | 0.02-6.42   |
| 2-Methylthreitol   | 2.34±3.95    | 0.33-18.79  | 2.88±2.97                      | 0.57-9.60   | 6.23±5.69       | 0.35-23.37  |
| 2-Methylerythritol   | 7.06±13.95   | 0.54-64.67  | 6.94±7.81                      | 1.08-23.58  | 13.49±12.23     | 0.48-47.62  |
| cis-2-Methyl-1,3,4-trihydroxy-1-butene                     | 0.87±1.25    | 0.15-6.06   | 2.00±2.56                      | 0.33-8.62   | 5.78±4.57       | 0.22-17.19  |
| 3-Methyl-2,3,4-trihydroxy-1-butene                         | 0.52±0.49    | 0.15-2.00   | 1.03±1.17                      | 0.23-4.08   | 2.40±1.91       | 0.18-7.31   |
| trans-2-Methyl-1,3,4-trihydroxy-1-butene                   | 1.28±1.25    | 0.15-5.08   | 5.25±5.59                      | 0.48-18.68  | 10.52±8.19      | 0.37-25.23  |
| 3-MeTHF-3,4-diols  | 0.18±0.06    | 0.15-0.34   | 0.21±0.07                      | 0.15-0.32   | 0.29±0.12       | 0.15-0.60   |
| ΣC5-Alkene triols  | 2.68±2.52    | 0.45-8.89   | 8.27±8.92                      | 1.20-31.37  | 18.71±13.14     | 0.78-40.08  |
| ΣIsoprene tracers (exclude triols)                         | 10.06±18.09  | 1.22-84.87  | 11.23±11.18                    | 1.93-35.70  | 22.32±18.94     | 1.17-77.09  |
| ΣIsoprene tracers  | 12.74±20.13  | 1.67-93.41  | 19.51±19.41                    | 3.14-67.07  | 41.03±29.71     | 1.95-117.17 |
| <i>Tracers for monoterpenes SOA (ng m<sup>-3</sup>)</i>    |              |             |                                |             |                 |             |
| 3-Hydroxyglutaric acid                                     | 3.40±2.09    | 0.72-9.14   | 6.11±5.42                      | 0.66-19.15  | 11.53±6.27      | 1.35-22.04  |
| 3-Hydroxy-4,4-dimethylglutaric acid                        | 0.53±0.12    | 0.42-0.93   | 0.71±0.30                      | 0.43-1.39   | 0.91±0.28       | 0.41-1.39   |
| 3-Methyl-1,2,3-butanetricarboxylic acid                    | 0.59±0.19    | 0.40-1.18   | 0.84±0.39                      | 0.45-1.76   | 1.28±0.52       | 0.42-2.14   |
| 3-Isopropylpentanedioic acid                               | 1.07±0.38    | 0.55-1.85   | 1.52±0.86                      | 0.51-3.46   | 2.57±1.52       | 0.61-4.86   |
| 3-Acetyl pentanedioic acid                                 | 0.82±0.23    | 0.45-1.19   | 1.13±0.55                      | 0.49-2.42   | 1.71±0.87       | 0.54-3.20   |
| Σ Monoterpenes tracers                                     | 6.41±2.75    | 2.63-13.49  | 10.31±7.33                     | 2.54-28.17  | 18.00±9.28      | 3.33-32.57  |
| <i>Tracers for β-caryophyllene SOA (ng m<sup>-3</sup>)</i> |              |             |                                |             |                 |             |
| β-Caryophyllinic acid                                      | 0.94±0.41    | 0.49-2.36   | 1.73±1.16                      | 0.75-3.99   | 2.33±1.21       | 0.80-5.82   |
| <i>Tracers for Naphthalene SOA (ng m<sup>-3</sup>)</i>     |              |             |                                |             |                 |             |
| Phthalic acid  | 2.26±1.38    | 0.80-5.17   | 4.97±3.30                      | 0.92-11.41  | 7.16±3.61       | 1.41-16.42  |
| <i>Dicarboxylic acids (ng m<sup>-3</sup>)</i>              |              |             |                                |             |                 |             |
| Succinic acid  | 2.10±1.63    | 0.65-6.23   | 4.56±4.80                      | 0.80-14.18  | 5.27±3.43       | 0.68-12.19  |
| Maleic acid  | 0.42±0.27    | 0.14-1.47   | 0.42±0.23                      | 0.14-0.84   | 0.36±0.18       | 0.15-0.78   |
| Malic acid   | 2.67±1.49    | 0.64-5.59   | 4.20±3.74                      | 0.60-13.12  | 8.10±4.12       | 1.33-13.86  |
| Glutaric acid  | 2.63±6.06    | 0.82-30.89  | 2.36±1.73                      | 0.79-4.99   | 2.85±1.53       | 0.67-6.05   |
| Citramalic acid  | 0.76±0.23    | 0.38-1.30   | 0.86±0.32                      | 0.38-1.48   | 1.23±0.47       | 0.52-2.00   |
| Terephthalic acid  | 9.28±7.49    | 2.16-31.86  | 30.21±27.20                    | 3.58-79.61  | 36.89±23.84     | 3.77-79.25  |
| Adipic acid  | 1.34±1.42    | 0.54-6.20   | 1.20±0.46                      | 0.64-2.21   | 1.48±0.66       | 0.67-3.08   |
| Pimelic acid   | 0.68±0.10    | 0.51-0.93   | 0.82±0.29                      | 0.52-1.47   | 0.99±0.35       | 0.52-1.94   |
| Oxalic acid (μg m <sup>-3</sup> )                          | 0.35±0.20    | 0.11-0.86   | 0.38±0.23                      | 0.09-0.72   | 0.54±0.21       | 0.29-0.94   |
| <i>Saccharides (ng m<sup>-3</sup>)</i>                     |              |             |                                |             |                 |             |
| Levogluconan   | 22.51±41.16  | 0.64-161.16 | 120.79±129.55                  | 3.21-362.74 | 128.52±140.39   | 8.64-474.15 |
| Meso-erythritol  | 0.11±0.10    | 0.03-0.43   | 0.29±0.25                      | 0.03-0.74   | 0.44±0.28       | 0.07-1.22   |
| Xylitol  | 0.29±0.11    | 0.21-0.69   | 0.50±0.28                      | 0.23-1.02   | 0.52±0.22       | 0.22-1.03   |
| Xylose   | 1.24±1.08    | 0.50-4.57   | 4.65±4.45                      | 0.58-13.34  | 5.34±4.31       | 0.81-16.12  |
| Galactose  | 1.82±2.02    | 0.37-9.97   | 3.31±1.97                      | 1.09-7.08   | 3.51±1.71       | 1.02-6.84   |
| Mannitol   | 0.16±0.04    | 0.12-0.26   | 0.21±0.07                      | 0.13-0.37   | 0.23±0.07       | 0.13-0.37   |
| Fructose   | 2.30±3.19    | 0.26-15.58  | 3.64±3.89                      | 0.38-13.41  | 4.32±2.54       | 1.65-9.32   |
| Galactosan   | 1.09±0.53    | 0.79-2.99   | 2.58±2.47                      | 0.84-7.20   | 2.68±2.40       | 0.88-7.99   |
| Sorbitol   | 1.45±0.37    | 1.14-2.54   | 1.55±0.28                      | 1.21-1.96   | 1.70±0.40       | 1.31-2.62   |
| Glucose  | 1.55±0.89    | 0.50-3.83   | 1.20±0.61                      | 0.40-2.07   | 1.51±0.92       | 0.52-3.29   |
| Sucrose  | 0.94±1.81    | 0.42-9.43   | 0.58±0.14                      | 0.42-0.91   | 0.57±0.08       | 0.45-0.76   |
| Arbitol  | 0.25±0.10    | 0.00-0.57   | 0.40±0.20                      | 0.22-0.78   | 0.42±0.17       | 0.22-0.85   |
| <i>Other compounds (ng m<sup>-3</sup>)</i>                 |              |             |                                |             |                 |             |

|  |            |            |            |            |            |            |
|--|------------|------------|------------|------------|------------|------------|
| 4-Nitrocatechol                                    | 0.90±0.12  | 0.78-1.35  | 1.30±0.62  | 0.84-2.75  | 1.55±0.83  | 0.85-4.00  |
| Cholesterol  | 1.29±0.25  | 0.94-1.81  | 1.30±0.28  | 1.01-1.93  | 1.20±0.27  | 0.95-1.89  |
| 1,2,3-Benzenetricarboxylic Acid                    | 1.23±0.67  | 0.47-2.46  | 2.25±1.34  | 0.63-4.70  | 3.97±2.54  | 0.54-9.50  |
| 1,2,4-Benzenetricarboxylic Acid                    | 1.77±1.28  | 0.47-6.17  | 3.32±2.34  | 0.88-6.77  | 5.16±3.30  | 0.73-12.54 |
| <i>Major ion (<math>\mu\text{g m}^{-3}</math>)</i> |            |            |            |            |            |            |
| Sulfate  | 11.43±5.98 | 3.28-30.32 | 13.02±9.25 | 1.49-29.25 | 17.35±5.20 | 8.90-29.29 |
| Nitrate  | 0.89±1.17  | 0.05-3.39  | 1.62±2.10  | 0.08-5.84  | 1.41±1.51  | 0.38-5.49  |
| Chloride   | 0.18±0.17  | 0.06-0.77  | 0.17±0.15  | 0.07-0.45  | 0.14±0.09  | 0.07-0.40  |
| Ammonia  | 2.05±0.91  | 0.47-4.12  | 2.26±1.48  | 0.30-4.36  | 2.99±0.72  | 1.82-4.69  |
| Potassium  | 0.11±0.07  | 0.03-0.36  | 0.29±0.17  | 0.05-0.49  | 0.40±0.22  | 0.15-0.94  |
| Magnesium  | 0.01±0.01  | 0.00-0.03  | 0.02±0.01  | 0.00-0.04  | 0.02±0.01  | 0.00-0.04  |
| Calcium  | 0.03±0.03  | 0.00-0.13  | 0.08±0.07  | 0.02-0.23  | 0.08±0.04  | 0.02-0.15  |
| Sodium   | 0.09±0.09  | 0.01-0.40  | 0.16±0.14  | 0.03-0.52  | 0.14±0.06  | 0.08-0.30  |

800

801 Table 2: PMF and TBM-resolved OCs, concentrations of gas pollutants, PM<sub>2.5</sub>, EC, OC, and major aerosol characteristics  
 802 under different meteorological conditions.

|   | Local (N=24)   |              | Long regional transport (N=10) |              | Regional (N=15) |                 | Annual (N=49) |              |
|---|--|--------------|--------------------------------|--------------|-----------------|-----------------|---------------|--------------|
|   | Average  | Range        | Average                        | Range        | Average         | Range           | Average       | Range        |
| PM <sub>2.5</sub> (µg m <sup>-3</sup> )                     | 24.11±9.99   | 10.04-49.28  | 32.23±14.81                    | 7.63-50.68   | 38.5±10.48      | 26.20-65.28     | 30.17±12.72   | 7.63-65.28   |
| EC (µgC m <sup>-3</sup> )                                   | 1.02±0.57  | 0.47-2.75    | 0.85±0.60                      | 0.14-2.10    | 1.14±0.45       | 0.50-2.12       | 1.02±0.54     | 0.14-2.75    |
| OC <sub>measured</sub>                                      | 2.94±1.11  | 1.61-5.75    | 4.16±2.53                      | 1.25-8.53    | 6.15±2.51       | 3.21-12.97      | 4.18±2.37     | 1.25-12.97   |
|   | <i>PMF apportioned OC (µgC m<sup>-3</sup>)</i>               |              |                                |              |                 |                 |               |              |
| SOC <sub>SOA</sub>  | 0.78±0.65  | 0.00-2.27    | 1.14±0.82                      | 0.18-2.72    | 1.75±0.75       | 0.65-3.29       | 1.15±0.82     | 0.00-3.29    |
| SOC <sub>SS</sub>   | 0.49±0.37  | 0.00-1.74    | 0.56±0.67                      | 0.00-1.81    | 0.82±0.38       | 0.24-1.65       | 0.60±0.46     | 0.00-1.81    |
| OC <sub>BB</sub><br>(POC <sub>BB</sub> +SOC <sub>BB</sub> ) | 0.26±0.63  | 0.00-2.34    | 1.97±2.26                      | 0.00-6.34    | 2.08±2.63       | 0.00-8.96       | 1.17±1.99     | 0.00-8.96    |
| OC <sub>Vehicle</sub>                                       | 0.49±0.46  | 0.00-2.07    | 0.30±0.42                      | 0.00-1.26    | 0.45±0.36       | 0.01-1.26       | 0.44±0.42     | 0.00-2.07    |
| OC <sub>Marine</sub>  | 1.00±0.63  | 0.04-2.97    | 0.23±0.19                      | 0.00-0.51    | 0.37±0.21       | 0.08-0.71       | 0.65±0.18     | 0.00-2.97    |
| OC <sub>Sea salt</sub>                                      | 0.10±0.11  | 0.00-0.53    | 0.25±0.33                      | 0.00-1.13    | 0.22±0.16       | 0.00-0.62       | 0.17±0.19     | 0.00-1.13    |
| SOC <sub>BB</sub>   | 0.09±0.21  | 0.00-0.79    | 0.66±0.76                      | 0.00-2.13    | 0.70±0.88       | 0.00-3.01       | 0.39±0.67     | 0.00-3.01    |
| SOC <sub>PMF</sub>  | 1.36±0.81  | 0.00-3.07    | 2.36±1.54                      | 0.33-4.78    | 3.27±1.18       | 1.63-5.53       | 2.15±1.37     | 0.00-5.53    |
| SOC <sub>PMF</sub> /OC (%)                                  | 43.0±16.8%   | 0.0%-66.5%   | 52.3±21.1%                     | 30.0%-85.3%  | 60.2±13.7%      | 36.2%-78.8%     | 50.2±18.2%    | 0.0%-85.3%   |
|   | <i>Tracer based method estimated OC (µgC m<sup>-3</sup>)</i> |              |                                |              |                 |                 |               |              |
| SOC <sub>bo</sub>   | 0.04±0.06  | 0.01-0.24    | 0.07±0.07                      | 0.01-0.23    | 0.14±0.12       | 0.01-0.49       | 0.08±0.09     | 0.01-0.49    |
| SOC <sub>Mono</sub>   | 0.14±0.06  | 0.06-0.29    | 0.22±0.16                      | 0.05-0.60    | 0.38±0.20       | 0.07-0.69       | 0.23±0.17     | 0.05-0.69    |
| SOC <sub>Carry</sub>  | 0.04±0.02  | 0.02-0.10    | 0.08±0.05                      | 0.03-0.17    | 0.10±0.05       | 0.03-0.25       | 0.07±0.05     | 0.02-0.25    |
| SOC <sub>Nap</sub>  | 0.06±0.04  | 0.02-0.13    | 0.13±0.09                      | 0.02-0.30    | 0.19±0.09       | 0.04-0.43       | 0.11±0.09     | 0.02-0.43    |
| SOC <sub>TBM</sub>  | 0.28±0.13  | 0.11-0.53    | 0.50±0.29                      | 0.12-1.06    | 0.81±0.35       | 0.15-1.53       | 0.49±0.34     | 0.11-1.53    |
| SOC <sub>TBM</sub> /OC                                      | 10.2±5.1%  | 3.8%-22.7%   | 13.0±4.6%                      | 5.3%-20.7%   | 13.4±4.3%       | 4.7%-19.6%      | 11.8±4.9%     | 3.8%-22.7%   |
|   | <i>Gas Pollutants and other aerosol characteristics</i>      |              |                                |              |                 |                 |               |              |
| O <sub>3_ave</sub> (ppb)                                    | 11.61±7.3  | 2.93-32.12   | 13.96±7.94                     | 2.86-26.92   | 20.64±8.74      | 2.88-31.84      | 14.85±8.69    | 2.86-32.12   |
| NO <sub>2_ave</sub> (ppb)                                   | 34.56±10.66  | 16.7-54.32   | 34.59±7.62                     | 21.74-42.85  | 42.98±7.10      | 32.72-60.37     | 37.15±9.76    | 16.70-60.37  |
| SO <sub>2_ave</sub> (µg m <sup>-3</sup> )                   | 4.14±2.92  | 0.7-10.38    | 3.81±1.88                      | 2.23-7.30    | 5.38±2.24       | 2.96-10.45      | 4.45±2.57     | 0.70-10.45   |
| O <sub>x</sub> (µg m <sup>-3</sup> )                        | 87.45±26.26  | 49.72-138.49 | 93.18±21.37                    | 61.66-125.79 | 122.39±17.70    | 69.54-145.90    | 99.31±27.42   | 49.72-145.90 |
| p[NO <sub>3</sub> ] (ppb h <sup>-1</sup> )                  | 1.25±0.96  | 0.30-4.17    | 1.36±0.94                      | 0.31-3.29    | 2.45±1.02       | 0.23-3.76       | 1.64±1.10     | 0.23-4.17    |
| NO <sub>2_ave</sub> (ppb)                                   | 0.05±0.04  | 0.01-0.18    | 0.06±0.04                      | 0.01-0.14    | 0.10±0.04       | 0.01-0.16       | 0.07±0.05     | 0.01-0.18    |
| H <sub>p</sub> <sup>+</sup> (M)                             | 1.72±1.04  | 0.02-3.78    | 2.66±1.50                      | 0.49-5.43    | 3.22±0.79       | 2.31-4.76       | 2.37±1.25     | 0.02-5.43    |
| pH  | (-0.20)±0.52   | (-0.58)-1.81 | (-0.31)±0.32                   | (-0.74)-0.31 | (-0.50)±0.10    | (-0.68)-(-0.36) | (-0.28)±0.42  | (-0.74)-1.81 |
| LWC (µg m <sup>-3</sup> )                                   | 66.64±46.51  | 2.68-184.71  | 42.88±28.80                    | 6.60-86.03   | 51.65±17.69     | 30.51-101.12    | 57.2±37.15    | 2.68-184.71  |

Formatted: Subscript

803

804 Table 3: Regression analysis (Pearson's R) of PMF and TBM-resolved SOC<sub>s</sub>, SO<sub>2</sub>, NO<sub>2</sub>, ozone (O<sub>3</sub>), particle acidity (H<sub>p</sub><sup>+</sup>),  
 805 total particle-phase liquid water content (LWC<sub>p</sub>), and sulfate \*\*: P<0.01; \*: P<0.05. Note: R>0.5 are bold.

|  | Pearson's R        |                     |                     |                    |                    |                   |                    |                   |                    |
|--|--------------------|---------------------|---------------------|--------------------|--------------------|-------------------|--------------------|-------------------|--------------------|
|  | SOC <sub>Iso</sub> | SOC <sub>Mono</sub> | SOC <sub>Cary</sub> | SOC <sub>Nap</sub> | SOC <sub>TBM</sub> | SOC <sub>BB</sub> | SOC <sub>SOA</sub> | SOC <sub>SS</sub> | SOC <sub>PMF</sub> |
| O <sub>3</sub> (ppb)                   | 0.374**            | .401**              | 0.011               | 0.246              | .374**             | -0.111            | <b>.502**</b>      | <b>.557**</b>     | .434**             |
| NO <sub>2</sub> (ppb)                  | .064               | <b>.516**</b>       | <b>.586**</b>       | <b>.528**</b>      | <b>.500**</b>      | .469**            | <b>.570**</b>      | 0.165             | <b>.627**</b>      |
| SO <sub>2</sub> (ppb)                  | 0.044              | 0.198               | .463**              | .296*              | 0.255              | .357*             | 0.035              | -0.052            | 0.179              |
| O <sub>x</sub> (μg m <sup>-3</sup> )   | 0.257              | <b>.600**</b>       | .433**              | <b>.535**</b>      | <b>.577**</b>      | 0.281             | <b>.707**</b>      | .445**            | <b>.711**</b>      |
| NO <sub>3</sub> (ppb)                  | .413**             | <b>.530**</b>       | 0.101               | .313*              | .480**             | -0.077            | <b>.637**</b>      | <b>.574**</b>     | <b>.538**</b>      |
| Sulfate (μg m <sup>-3</sup> )          | .287*              | <b>.610**</b>       | .405**              | <b>.506**</b>      | <b>.579**</b>      | 0.23              | <b>.646**</b>      | <b>.886**</b>     | <b>.799**</b>      |
| H <sub>p</sub> <sup>+</sup> (M)        | 0.249              | .334*               | .391**              | .388**             | .395**             | .400**            | 0.164              | 0.24              | .376**             |
| LWC <sub>p</sub> (μg m <sup>-3</sup> ) | -0.18              | 0.18                | 0.115               | 0.209              | 0.113              | 0.003             | .413**             | .438**            | .397**             |

Formatted Table

806 Table 4: Results of multivariate linear analysis of PMF and TBM-resolved SOC<sub>s</sub>, NO<sub>x2</sub>, NO<sub>3</sub>, sulfate, particle acidity (H<sub>p</sub><sup>+</sup>),  
 808 and total particle-phase liquid water content (LWC<sub>p</sub>). \*\*: P<0.01; \*: P<0.05. Note: significant regressions are bold.

| -                                      | normalized β-coefficient |                     |                     |                    |                    |                   |                    |                   |                    |
|--|--------------------------|---------------------|---------------------|--------------------|--------------------|-------------------|--------------------|-------------------|--------------------|
|  | SOC <sub>Iso</sub>       | SOC <sub>Mono</sub> | SOC <sub>Cary</sub> | SOC <sub>Nap</sub> | SOC <sub>TBM</sub> | SOC <sub>BB</sub> | SOC <sub>SOA</sub> | SOC <sub>SS</sub> | SOC <sub>PMF</sub> |
| NO <sub>2</sub> (ppb)                  | -0.013                   | <b>0.351**</b>      | <b>0.660**</b>      | <b>0.445**</b>     | <b>0.383**</b>     | <b>0.639**</b>    | 0.270*             | <b>-0.303**</b>   | <b>0.373**</b>     |
| NO <sub>3</sub> (ppb)                  | 0.309                    | 0.174               | <b>-0.382**</b>     | -0.077             | 0.101              | <b>-0.509**</b>   | <b>0.384**</b>     | <b>0.234**</b>    | 0.059              |
| Sulfate (μg m <sup>-3</sup> )          | 0.343                    | 0.417*              | 0.240               | 0.202              | 0.393*             | 0.083             | 0.303              | <b>0.913**</b>    | <b>0.530**</b>     |
| H <sub>p</sub> (M)                     | -0.138                   | 0.047               | 0.378*              | 0.348*             | 0.129              | <b>0.503**</b>    | -0.053             | -0.189*           | 0.151              |
| LWC <sub>p</sub> (μg m <sup>-3</sup> ) | -0.392                   | -0.135              | -0.091              | 0.071              | -0.171             | -0.073            | 0.125              | 0.096             | 0.071              |

| -                                      | normalized β-coefficient |                     |                    |                     |                    |                     |                     |                    |                     |
|--|--------------------------|---------------------|--------------------|---------------------|--------------------|---------------------|---------------------|--------------------|---------------------|
|  | SOC <sub>SS-</sub>       | SOC <sub>SOA-</sub> | SOC <sub>BB-</sub> | SOC <sub>PMF-</sub> | SOC <sub>Iso</sub> | SOC <sub>Mono</sub> | SOC <sub>Cary</sub> | SOC <sub>Nap</sub> | SOC <sub>TBM-</sub> |
| O <sub>x</sub> (μg m <sup>-3</sup> )   | <b>-0.453**</b>          | 0.355               | <b>1.08**</b>      | <b>0.59**</b>       | -0.091             | <b>0.439*</b>       | <b>1.045**</b>      | <b>0.739**</b>     | <b>0.537*</b>       |
| NO <sub>3</sub> (ppb)                  | <b>0.497**</b>           | <b>0.186</b>        | <b>-1.159**</b>    | -0.289*             | 0.375              | -0.066              | <b>-0.999**</b>     | -0.519*            | -0.204              |
| Sulfate (μg m <sup>-3</sup> )          | <b>0.877**</b>           | 0.334*              | 0.164              | <b>0.576**</b>      | 0.339              | 0.457*              | 0.323               | 0.258              | 0.439*              |
| H <sub>p</sub> (M)                     | -0.141                   | -0.091              | <b>0.386**</b>     | 0.087               | -0.127             | 0.001               | 0.265               | 0.268              | 0.072               |
| LWC <sub>p</sub> (μg m <sup>-3</sup> ) | 0.122                    | 0.116               | -0.166             | 0.029               | -0.369             | -0.14               | -0.166              | 0.1                | -0.194              |

Formatted Table

Formatted: Centered

Formatted: Font: Bold

Formatted: Font: Bold

Formatted: Font: Bold

809